



Regionally consistent Western North America paleomagnetic directions from 15 to 35 ka: Assessing chronology and uncertainty with paleosecular variation (PSV) stratigraphy

Brendan T. Reilly^{a,*}, Joseph S. Stoner^a, Robert G. Hatfield^a, Mark B. Abbott^b, David W. Marchetti^c, Darren J. Larsen^d, Matthew S. Finkenbinder^e, Aubrey L. Hillman^f, Stephen C. Kuehn^g, Clifford W. Heil Jr.^h

^a College of Earth, Ocean, and Atmospheric Sciences, Oregon State University, Corvallis, OR, 97331, USA

^b Geology and Environmental Science, University of Pittsburgh, PA, 15260, USA

^c Geology Program, Western State Colorado University, Gunnison, CO, 81230, USA

^d Department of Geology, Occidental College, Los Angeles, CA, 90041, USA

^e Environmental Engineering and Earth Sciences, Wilkes University, Wilkes-Barre, PA, 18766, USA

^f Department of Environmental Sciences, School of Geosciences, University of Louisiana at Lafayette, Lafayette, LA, 70504, USA

^g Department of Physical Science, Concord University, Athens, WV, 24712, USA

^h Graduate School of Oceanography, University of Rhode Island, 215 South Ferry Road, Narragansett, RI, 02882, USA

ARTICLE INFO

Article history:

Received 17 August 2018

Received in revised form

11 October 2018

Accepted 12 October 2018

Keywords:

Pleistocene

Paleolimnology

North America

Paleomagnetism

Paleomagnetic secular variation

Chronostratigraphic modeling

Quaternary geochronology

Radiocarbon

Computed tomography (CT)

ABSTRACT

New Paleomagnetic Secular Variation (PSV) data from Fish Lake, Utah, USA, along with previously published regional records, allow us to build an independently dated Western North America PSV stack (WNAM17) from about 35 to 15 ka that quantifies dating and paleomagnetic uncertainties. In February 2014, we recovered a composite 11-m-long sediment record from Fish Lake, Utah that retrieved glacially influenced and post-glacial sediments. Computed tomography (CT) scans and magnetic susceptibility were used to build a precise depth scale, while radiocarbon dating of terrestrial macrofossils and tephrostratigraphy provide tight age-control. Glacially influenced sediments have well-defined characteristic remanent magnetizations with all maximum angular deviation values $< 5^\circ$, resolving a record of Late Pleistocene PSV. Comparison to the PSV records at Bear Lake, Utah/Idaho, USA and Besette Creak, British Columbia, Canada, which also contain terrestrial material radiocarbon age-control points, allow us to develop the WNAM17 PSV stack which considers both dating and magnetic acquisition uncertainties. We utilize a regional PSV chronostratigraphic modeling approach to assign chronology and uncertainty to the PSV signal and to evaluate the fidelity of age-control points at the site level that are difficult to objectively evaluate otherwise. The greatest strength of our age-depth model is that by approaching chronostratigraphy from a regional perspective, assuming a common geomagnetic signal, we can address sources of geologic uncertainty that would be difficult to quantify using only one site. We illustrate the potential stratigraphic opportunities using the WNAM17 PSV template through assessing the timing of paleoenvironmental and paleomagnetic events in Western North America, including the timing of glaciations in the Fish Lake and Bear Lake catchments and the stratigraphic context for the Late Pleistocene geomagnetic excursion recorded at Mono Lake.

© 2018 Elsevier Ltd. All rights reserved.

1. Introduction

Well-dated and high resolution sedimentary records of

geomagnetic paleosecular variation (PSV) have both transformed our knowledge of geomagnetic field behavior on millennial time-scales and provided a stratigraphic method independent of climate correlation with wide-ranging application, including improvement of paleoceanographic and paleoclimate chronologies (Darby et al., 2012; Stoner et al., 2007), direct marine and terrestrial comparisons (Ólafsdóttir et al., 2013), and assessment of reservoir age

* Corresponding author.

E-mail address: breilly@coas.oregonstate.edu (B.T. Reilly).

changes through time (Wüdsch et al., 2016). PSV describes the general spatial and temporal variability of the Earth's magnetic field and typically is used in reference to directional variations during periods of stable polarity (Johnson and McFadden, 2007; Lund, 2007). While a number of stacks have been developed to define regional templates for PSV in the Holocene (Barletta et al., 2010; Snowball et al., 2007; Thompson and Turner, 1979; Walczak et al., 2017; Zheng et al., 2014), Late Pleistocene paleomagnetic stacks have mostly focused on regional or global relative paleointensity (RPI) changes (Laj et al., 2004; Nowaczyk et al., 2013; Stoner et al., 2002). This is likely due, in part, to the difficulty of establishing continuous, well-dated, and high-resolution records in Late Pleistocene sediments that can also resolve the amplitude and timing of centennial to millennial directional changes characteristic of PSV.

High-magnitude climate variability during the late Pleistocene often led to large changes in environmental conditions and depositional processes in sedimentary basins. Such changes can result in variations of magnetic remanence acquisition efficiency across lithologic transitions and complicate continuous reconstructions of RPI (e.g. Mazaud, 2006; Schwartz et al., 1996; Tauxe, 1993). Paleomagnetic directions are often less impacted by these lithologic variations and can be directly compared between archives without having to make scaling factor assumptions. This provides the opportunity to reconstruct past field morphology changes using approaches that integrate discontinuous PSV records and chronologies, such as efforts to extend the Scandinavian PSV reference curve through the last deglacial interval (Lougheed et al., 2014).

PSV has been central to a number of Western North America Late Pleistocene studies, and while many PSV records appear to have regionally consistent features (Benson et al., 2003b; Liddicoat, 1992; Negrini et al., 1984), the lack of strong independent chronologies has led researchers to use far field correlations to well-dated Western North Atlantic records (Benson et al., 2011, 1998; Lund et al., 2017) or rely on regional correlations to records with poorly constrained chronologies (Clague et al., 2003).

We present new PSV data from Fish Lake, Utah (UT), which, when combined with previously published PSV data from Bear Lake, Utah/Idaho (Heil et al., 2009), and Bessette Creek, British Columbia (Turner et al., 1982), offers a step forward in building a well-defined and independently dated PSV reference curve that considers chronologic and magnetic uncertainties from ~35 to 15 ka (Fig. 1). These sites are positioned on the southern margin of a region of high radial magnetic flux at the core-mantle boundary, or 'flux lobe', as recognized in the *gufm1* historical geomagnetic field reconstruction (Jackson et al., 2000). This high flux region is likely persistent or recurrent on longer timescales (Bloxxham, 2002; Stoner et al., 2013). Evidence from independently dated Holocene records from Western North America suggests that the timing of high-amplitude PSV features, particularly inclination, are largely consistent across the mid-latitude Western United States (Hanna and Verosub, 1989, 1988; Lund, 1996), Northeast Pacific (Walczak et al., 2017), and the Western Canadian Arctic (Barletta et al., 2008; St-Onge and Stoner, 2011). Global comparisons of these Holocene directional records suggest that high-amplitude features that occur on roughly millennial timescales are a reflection of large-scale geomagnetic field dynamics related to oscillation of intensity between the North American and other Northern Hemisphere flux lobes (Nilsson et al., 2011, 2010; Stoner et al., 2013; Walczak et al., 2017). These PSV features provide a stratigraphic context for both paleoenvironmental and paleomagnetic events recognized in Western North American sediments that can be integrated with the radiocarbon timescale to provide greater accuracy than is possible with radiometric methods alone.

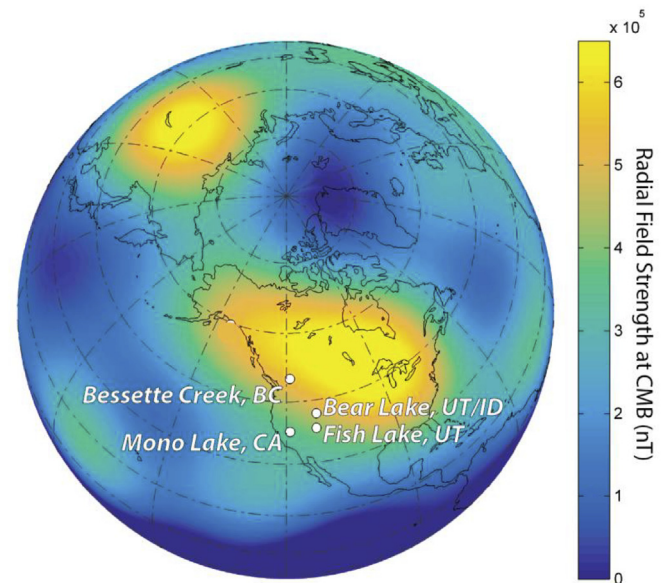


Fig. 1. Radial Field Strength at the Core Mantle Boundary (CMB) from 1590 to 1990 time averaged field, based on the historical reconstruction *gufm1* (Jackson et al., 2000), with locations of mid-latitude western North American PSV sites discussed in the text, including Fish Lake, Utah, a British Columbia outcrop at Bessette Creek (Turner et al., 1982), Bear Lake on the Idaho/Utah border (Heil et al., 2009), and Mono Lake in California (Lund et al., 1988).

2. Fish Lake, Utah

Fish Lake, Sevier County, Utah (38.54° N, 111.71° W; elevation 2700 m), a common name for North American lakes including the important Holocene paleomagnetic site, Fish Lake, Oregon (Verosub et al., 1986), is the largest natural mountain lake in the state of Utah, USA. Lake dimensions are roughly 5 km by 1.7 km, with a maximum water depth of ~37 m. The lake basin is located in a northeast-southwest trending graben in the high plateau of Utah, a transitional region between the Colorado Plateau and the Basin and Range (Bailey et al., 2007). Glacial geology and lake bathymetry suggest glaciers drained from the Fish Lake High-top plateau (elevation 3546) to the Fish Lake basin without overrunning the lake during the last and penultimate glaciations (Marchetti et al., 2011), providing an opportunity to recover a continuous record of Late Pleistocene glacial activity, paleoenvironmental conditions, and paleomagnetism. ³He cosmogenic exposure ages of moraine boulders suggest local last glacial maximum ice extent occurred ~21 ka with a possible readvance or standstill at ~15–18 ka (Marchetti et al., 2011).

3. Methods and materials

3.1. Sediment cores and computed tomography (CT) scans

Sediment cores were collected in a series of ~2-m-long drives, using a 9 cm diameter UWITEC system deployed from the frozen surface of Fish Lake, UT in February 2014. Three adjacent holes were cored, with two drives recovered from Hole A14, and five drives recovered from both Holes B14 and C14 (Fig. 2). During the coring effort, a MS3 Bartington magnetic susceptibility meter with 100 mm diameter MS2C loop sensor was used to measure magnetic susceptibility of each drive to ensure overlap and inform coring decisions.

Before being split, all sediment cores were scanned on the Oregon State University (OSU) College of Veterinary Medicine Toshiba Aquillon 64 Slice medical computed tomography (CT)

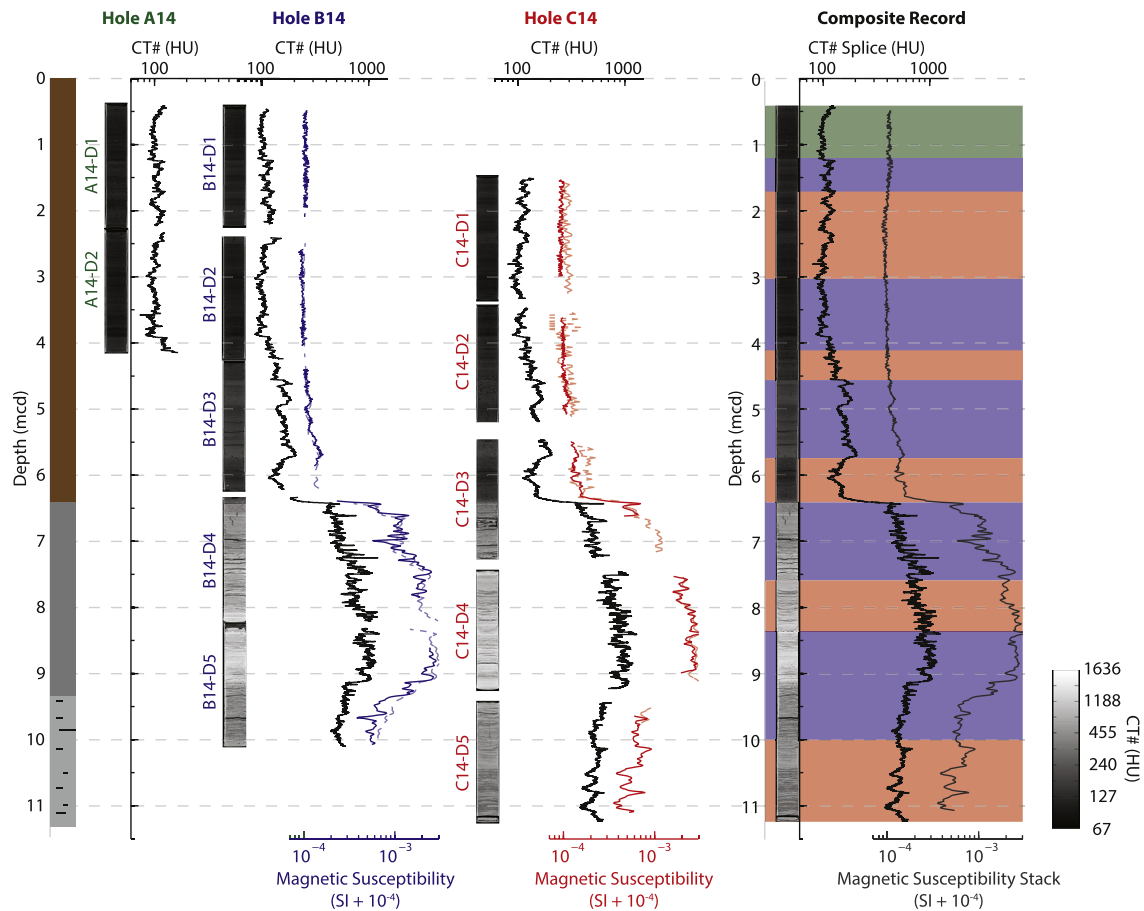


Fig. 2. Simplified lithologic log, CT scan slices (3.5x horizontal exaggeration), CT numbers, and magnetic susceptibility for Fish Lake, Utah cores recovered during the 2014 field season on the meters composite depth scale (Table 1). The simplified lithologic changes (from top to bottom) of brown organic-rich mud, to massive gray silty clay, to gray silty clay with faint black laminations. Magnetic susceptibility data are offset by 10^{-4} SI so that they can be plotted on a log scale, as some values measured in the upper 6.5 mcd are negative, and include u-channel (dark continuous line) and field whole round (light dashed line) measurements. The field whole round data are arbitrarily scaled by 40% to match the u-channel data. A composite record is made by splicing the CT scans together (Table 1) and stacking all u-channel magnetic susceptibility data on the mcd scale. Shading for the composite record indicates the hole used for each interval in the CT splice (Green = A14; Blue = B14; Red = C14). Note CT image grayscale has non-linear scaling to account for large density differences between lithologic units. (For interpretation of the references to color in this figure legend, the reader is referred to the Web version of this article.)

scanner at 120 kV. A “sharp” algorithm was used to produce 2 mm thick coronal slices, which have an effective resolution of 0.5×0.5 mm within the plane of each slice. SedCT MATLAB tools were used to extract downcore CT number profiles, which largely reflect changes in sediment density, and CT slice images (Reilly et al., 2017). A composite record splice was developed for the CT scans, based on the meters composite depth (mcd) scale (developed by correlation of the CT scan number profiles and u-channel magnetic susceptibility as discussed below) and identification of tie points that correlate at the sub-cm scale in the CT number profiles (Table 1).

Cores from Holes B14 and C14 were split at the OSU Marine and Geology Repository. Three principle lithologies were observed: a low density brown organic mud in the upper 6.35 mcd, a massive gray silty clay from 6.35 mcd to about 9.34 mcd, and a gray mud with faint black laminations below ~9.34 mcd. These lithologic units correspond to major density changes, as observed in the CT scans, and are associated with large changes in the concentration of ferrimagnetic minerals, as reflected by measurements of magnetic susceptibility (Fig. 2).

3.2. Sediment magnetic measurements

U-channel samples, $\sim 2 \text{ cm} \times 2 \text{ cm}$ x up to 150 cm u-shaped

plastic containers with a plastic lid, were sampled from the center of the working halves of Fish Lake, UT cores from Holes B14 and C14. Because the UWITEC cores were commonly longer than 150 cm, u-channels were preferentially sampled away from the tops and bottoms of core sections to avoid potentially compressed or disturbed sediments and to ensure a complete sampling of the entire stratigraphy based on the field magnetic susceptibility correlations.

The sediment natural remanent magnetization (NRM) and anhysteretic remanent magnetization (ARM) were measured at the OSU Paleo and Environmental Magnetism Lab on a 2G Enterprises™ model 755–1.65UC superconducting rock magnetometer (SRM™) with inline alternating field (AF) coils optimized for u-channel samples. Measurements were made every 1 cm with a 10 cm leader and trailer; however, the effective resolution is the integrated remanent magnetization within the 7.6 cm full width at half maximum (FWHM) response function of the magnetometer (see Oda and Xuan, 2014 for detailed discussion of the OSU system). In this study SRM data from the leader, trailer, and 5 cm at either end of each u-channel are not reported in the results but are necessary for the deconvolution experiments discussed below.

The NRM of Core B14-D1 was measured before and after peak AF demagnetization every 5 mT from 10 to 70 mT and at 80 mT (15 measurements). Due to this sample's weak magnetization and

Table 1
Depth table for 2014 field season fish lake, UT UWITEC cores.

Hole	Drive	Difference End Cap/Sediment Start (m)	U-Channel Start in Section (m) ^a	mcd Offset (m) ^a	Section# in Splice	Top Section Depth (m) ^a	Bottom Section Depth (m) ^a
A14	1	0.03	–	0.41	1	0	0.80
	2	0.04	–	2.33	–	–	–
B14	1	0.04	0.00	0.46	2	0.75	1.25
	2	0.02	0.15	2.41	4	0.62	1.70
	3	0.05	0.08	4.30	6	0.26	1.44
	4	0.02	0.02	6.35	8	0.06	1.24
	5	0.02	0.34	8.25	10	0.12	1.76
C14	1	0.03	0.00	1.51	3	0.20	1.52
	2	0.03	0.13	3.47	5	0.64	1.09
	3	0.01	0.00	5.47	7	0.27	0.94
	4	0.01	0.06	7.45	9	0.15	0.92
	5	0.02	0.18	9.44	11	0.55	1.79

^a Measured from start of sediment in core liner.

demagnetization behavior, the NRM of the other nine u-channels were measured every 2.5 mT from 10 to 40 mT, every 5 mT from 45 to 60 mT and every 10 mT from 70 to 80 mT (20 measurements). Following demagnetization of the NRM, an ARM was applied using a 100 mT peak AF and 0.05 mT biasing field. The ARM was measured before and after peak AF demagnetization every 5 mT from 10 to 70 mT and at 80 mT (15 measurements).

U-channel magnetic susceptibility was measured every 1 cm on a motion-controlled u-channel track built at OSU with a Bartington MS3 meter attached to an MS2C loop sensor with an internal diameter of 36 mm. Reported values are the mean of three repeat measurements. A magnetic susceptibility stack was created from u-channel data on their composite depth scale, after trimming the top and bottom 3 cm to account for edge-effects of the Bartington Loop sensor. The stack was created at 1 cm composite depth intervals using a weighted running mean with weighting based on a narrow Gaussian function filter with a FWHM of 1 cm.

3.3. Processing and stacking magnetic data

Flux jumps in the SRM data were monitored and corrected using UPmag MATLAB tools (Xuan and Channell, 2009) and Characteristic Remanent Magnetization (ChRM) directions, inclination and declination, were calculated using the PCA method (Kirschvink, 1980). For intervals with very well defined ChRMs (B14 Drives 4 and 5 and C14 Drives 4 and 5), deconvolution experiments were performed with UDecon MATLAB Tools (Oda and Xuan, 2014; Xuan and Oda, 2015).

After removing sections based on quality criteria (discussed in RESULTS) and rotating declinations first to a zero mean and then modified based on agreement between overlapping drives, paleomagnetic directions were stacked every 1 cm by calculating a weighted running vector mean with weighting defined by a 5 cm FWHM Gaussian function filter after applying the error propagation technique described below. For the deconvolved Fish Lake, UT data, a 3 cm FWHM Gaussian function filter was used. Error related to measurement precision was propagated by scaling maximum angular deviation (MAD) values to 95% confidence intervals (after Khokhlov and Hulot, 2016) and selecting 1000 random values from a normal distribution with standard deviations (σ) for inclination and declination calculated from the 95% confidence interval (after Donadini et al., 2009). At each stack depth (D_s), each set of 1000 random values for each paleomagnetic measurement whose composite depth (D_{cd}) were within $\pm 5\sigma$ (σ is the standard deviation of the Gaussian function and is equal to about 42% of the FWHM width) were binned and weighted using the Gaussian distribution function:

$$g(D_i) = \exp\left(-\frac{D_i^2}{2\sigma^2}\right), \text{ Where } D_i = D_s - D_{cd} \quad (1)$$

The vector mean and Fisher statistics (Fisher, 1953) were calculated for the binned data at each stack depth, using the weighted vector magnitude (R) calculated by:

$$R = \sqrt{\left(\sum_{i=1}^n g(D_i)x_i\right)^2 + \left(\sum_{i=1}^n g(D_i)y_i\right)^2 + \left(\sum_{i=1}^n g(D_i)z_i\right)^2} \quad (2)$$

Where n is equal to the number of data in each bin and x_i , y_i , z_i are the east-west, north-south, and vertical components, respectively, of the i th binned value. The weighted mean component directions are calculated by:

$$\bar{x} = \frac{\sum_{i=1}^n g(D_i)x_i}{R} \quad (3)$$

$$\bar{y} = \frac{\sum_{i=1}^n g(D_i)y_i}{R} \quad (4)$$

$$\bar{z} = \frac{\sum_{i=1}^n g(D_i)z_i}{R} \quad (5)$$

Which allows the mean inclination and declination to be calculated by the standard method. The Fisher statistic precision parameter (κ) and α_{95} are approximated by:

$$\kappa = \frac{(N-1)}{(N-R)}, \text{ Where } N = \sum_{i=1}^n g(D_i) \quad (6)$$

$$\alpha_{95} = \frac{140}{\sqrt{\kappa C}} \quad (7)$$

Where C is equal to the number of cores that contribute to the bin and have a sum Gaussian weight for their measurements greater than one. We choose to normalize by the number of cores rather than the number of measurements used because the u-channel measurements are an integration of the magnetometer response function and are not independent measurements (as discussed above).

3.4. Additional regional records

For our regional comparison, we use paleomagnetic data from Bear Lake on the Utah and Idaho border from Heil et al. (2009) and the Bessette Creek Outcrop, British Columbia, originally studied by Oberg and Evans (1977) and later studied in detail by Turner et al. (1982) (Fig. 1). Sampling and paleomagnetic methods for these locations can be found in their original studies. While we use the complete Bessette Creek record, we focus only on the 9.75–25 m interval in Bear Lake, due to the excellent agreement between inclination in the BL00-1D and 1E Holes in this interval documented by Heil et al. (2009) and more ambiguous relationship above and below that.

3.5. Age control

Terrestrial macrofossil material, including charcoal, wood, and a seed, were used for radiocarbon dating of Fish Lake, UT sediments (Table 2). Bulk sediment samples were disaggregated with 7% H₂O₂ and sieved using a 125 µm stainless steel screen. The remaining material on the sieve was examined and macrofossil material isolated using a fine detail paint brush. Macrofossils were pretreated using a standard acid-base-acid pretreatment (Abbott and Stafford, 1996) before being combusted and reduced to graphite for AMS radiocarbon measurements at the Keck Carbon Cycle Accelerator Mass Spectrometer Laboratory at the University of California, Irvine. All radiocarbon samples were calibrated using MatCal (Lougheed and Obrochta, 2016) and the IntCal13 calibration curve (Reimer et al., 2013).

Five sediment samples were prepared for tephra analysis. Each sample was wet sieved, separated at a density of 2.5 g/cm³ using a solution of lithium heteropolytungstates, mounted in epoxy, polished to a 0.3 µm final grit, and carbon coated. Following Kuehn

(2016), geochemical analyses for 11 major and minor elements (SiO₂, TiO₂, Al₂O₃, FeO, MnO, CaO, Na₂O, K₂O, P₂O₅, and Cl) were performed at Concord University on an ARL-SEM-Q electron microprobe automated by Probe for EPMA software using one large-area energy-dispersive spectrometer (EDS) for Si and Al and four wavelength-dispersive spectrometers (WDS) for all other elements. Analytical conditions were 14 kV accelerating voltage, 10 nA beam current, and 4 to 10 µm diameter spot. A time-dependent intensity correction was applied as needed for Na, and water-by-difference was incorporated into the X-ray matrix corrections. Mean atomic number modeled X-ray backgrounds were used for all WDS elements with a blank correction to enhance minor/trace level accuracy. Lipari ID3506 (rhyolite), BHVO-2g (basalt), and NKT-1g (nephelinite) reference glasses were included in each analytical session (Kuehn et al., 2011). Following analysis, representative backscatter electron images were collected for the tephra grains.

Three of the five tephra layers observed in cores were matched to the Tabernacle Hill, Pavant Butte, and Pony Express tephra layers identified in the Lake Bonneville Basin (Oviatt and Nash, 1989, 2014) based on major and minor trace metal chemistry and stratigraphic relationships (Tables 2 and 3; Supplementary Dataset). Each of the samples contains a major elemental population along with tephra grains of multiple other compositions, suggesting a relatively high background level of reworked tephra grains in the lake sediments. Sample B14-D5 91.5 cm (CU1344) is a strong match to the approximately 20 ¹⁴C ka basaltic Pony Express tephra described by Oviatt and Nash (2014). Samples B14-D4 61 cm (CU1342) and B14-D4 91.5 cm (CU1343) contain compositionally indistinguishable basaltic glass compositions that compare closely to the ~15.6 ¹⁴C ka Pavant Butte and ~14.4 ¹⁴C ka Tabernacle Hill tephra described by Oviatt and Nash (1989), which we assign based on their stratigraphic order. Sample B14-D4 23 cm (CU1341)

Table 2
Age control points.

Core	Section Depth Interval (cm)	Composite Depth Midpoint (m)	Depth in BL00, Bear Lake (m)	Material	UCIAMS#/Lab#	¹⁴ C age (BP) ±	Ref.
Fish Lake, Utah							
B14-D1	89–90	1.355	–	Charcoal	141387	2455	20 This Study
C14-D1	31–33	1.830	–	Wood	141379	2890	20
C14-D1	174–175	3.255	–	Charcoal	141380	4585	50
C14-D2	55.5–56.5	4.030	–	Wood	141381	5840	25
C14-D2	111.5–112.5	4.590	–	Wood	141382	6630	80
C14-D2	136–137.5	4.838	–	Charcoal	141383	7940	25
C14-D2	165–168	5.135	–	Charcoal	141384	9150	30
B14-D3	151–152	5.815	–	Wood	141388	11270	60
C14-D3	40–41	5.875	–	Seed	141385	11325	40
C14-D3	60–61	6.075	9.21	Plant Material	152063	11760	250
B14-D4	61	6.960	12.08	Tephra Correlation (Tabernacle Hill)	–	14400	100
B14-D4	91.5	7.265	12.84	Tephra Correlation (Pavant Butte)	–	15650	350
B14-D5	91.5	9.165	17.54	Tephra Correlation (Pony Express)	–	20160	254
C14-D5	125–126	10.695	20.00	Wood	152064	24300	2800
C14-D5	136–139	10.815	20.15	Wood	141286	28200	2100
Bear Lake, Utah/Idaho							
BL96-2-2D	7	10.05 ^a	10.05	Pollen Extract	WW-1774	12710	50 Colman et al., 2009
BL96-2-2D	8	10.08 ^a	10.08	Pollen Extract	WW-2602	12545	90
BL96-3-3E	15	16.72 ^a	16.72	Pollen Extract	WW-2606	22150	210
BL00-1D-6H2	109–110	18.00	18.00	Pollen Extract	WW-6452	24280	110
BL00-1D-7H1	19–20	18.59	18.59	Pollen Extract	WW-6453	23340	100
Bessette Creek, British Columbia							
Outcrop	19.82	18.25 ^b	16.26	Moss	GSC-913	19100	240 Westgate and
Outcrop	6.90	6.90	20.21	Peat	GSC-1945	25400	270 Fulton, 1975
Outcrop	4.50	4.50	21.19	Wood	GSC-1953	25300	320
Outcrop	1.25	1.25	23.26	Peat	GSC-1938	31100	480
Outcrop	0.00	0.00	24.06	Bark	GSC-2031	31200	900

^a Correlation to BL00 depth scale based on Table 3 of Colman et al. (2009).

^b Adjusted depth scale of Turner et al. (1982), after removing gravel layers.

Table 3

Summary of geochemical data for major tephra glass populations, normalized to 100% totals. FeO_T is total iron oxide reported as FeO (Fe²⁺), some materials may contain significant Fe³⁺ (Fe₂O₃); n = number of analyses; S.C. = similarity coefficient; Pavant Butte and Tabernacle Hill tephra glass compositions from Oviatt and Nash (1989); Pony Express glass composition from Oviatt and Nash (2014). Table with complete data, including outliers and reference glass are available as a supplementary dataset.

Sample		SiO ₂	TiO ₂	Al ₂ O ₃	FeO _T	MnO	MgO	CaO	Na ₂ O	K ₂ O	P ₂ O ₅	Cl	n	S.C.
CU1341 - Core B14-D4 23 cm	Mean	71.69	0.68	13.78	2.41	0.06	0.29	0.80	3.35	6.78	0.10	0.07	13	
	StDev	0.73	0.04	0.34	0.13	0.01	0.03	0.09	0.38	0.25	0.02	0.01		
CU1342- Core B14-D4 61 cm	Mean	50.89	1.95	15.55	12.08	0.21	5.28	8.69	3.57	1.32	0.45	0.03	28	
	StDev	0.52	0.07	0.39	0.61	0.02	0.46	0.41	0.22	0.11	0.04	0.01		
Pavant Butte tephra (L-2)		51.40	1.74	15.82	12.19	0.19	5.00	8.55	3.33	1.34	0.34	0.02		0.97
Tabernacle Hill tephra (TH-3A)		50.56	1.82	15.69	11.69	0.18	5.34	9.62	3.32	1.28	0.49	0.02		0.96
CU1343 - Core B14-D4 91.5 cm	Mean	50.86	1.91	15.68	12.11	0.21	5.22	8.76	3.48	1.29	0.45	0.04	26	
	StDev	0.36	0.06	0.29	0.49	0.03	0.44	0.42	0.18	0.10	0.04	0.01		
Pavant Butte tephra (80–15)		51.19	1.66	15.83	11.82	0.18	5.32	8.93	3.37	1.29	0.34	0.02		0.98
Tabernacle Hill tephra (TH-3A)		50.56	1.82	15.69	11.69	0.18	5.34	9.62	3.32	1.28	0.49	0.02		0.97
CU1344 - Core B14-D5 91.5 cm	Mean	51.08	1.69	15.57	10.13	0.18	6.56	10.29	3.25	0.91	0.31	0.03	36	
	StDev	0.21	0.05	0.15	0.20	0.02	0.15	0.13	0.17	0.04	0.02	0.02		
Pony Express tephra (SK-2)		50.79	1.71	15.62	10.18	0.19	6.52	10.48	3.18	0.90	0.33	0.11		0.99
CU1345 - Core C14-D3 116.5 cm	Mean	50.73	1.97	15.76	11.66	0.20	5.35	9.09	3.52	1.25	0.45	0.03	13	
	StDev	0.24	0.11	0.21	0.36	0.03	0.33	0.32	0.29	0.08	0.04	0.01		
Pavant Butte tephra (PBN-SW)		51.26	1.78	15.71	11.48	0.16	5.37	9.22	3.31	1.27	0.35	0.02		0.98
Tabernacle Hill tephra (TH-3A)		50.56	1.82	15.69	11.69	0.18	5.34	9.62	3.32	1.28	0.49	0.02		0.98

contains a rhyolitic major population of unidentified origin. Traces of glass of similar composition are present in all the other samples, suggesting that this may represent reworked material. Sample C14-D3 116.5 (CU1345) contains a lower abundance of tephra grains than the other samples with a major population that could be correlative to either the Pavant Butte or Tabernacle Hill tephra.

Previously published pollen extract radiocarbon dates from Bear Lake cores BL96-2, BL96-3, and BL00-1D (Colman et al., 2009, 2006) and various terrestrial radiocarbon samples from the Bessette Creek Outcrop (Westgate and Fulton, 1975) that cover the Late Pleistocene were also used in this study after calibration using MatCal (Lougheed and Obrochta, 2016) and the IntCal13 calibration curve (Reimer et al., 2013). We follow the recommendation of Colman et al. (2009) for which radiocarbon samples to include and reject in Bear Lake and transfer depths to the BL00 depth scale using Table 3 in that publication.

4. Results

4.1. Fish Lake, Utah natural and laboratory remanent magnetizations

NRM intensities are relatively weak, typically between 10^{-4} and 10^{-3} A/m, in the low density brown organic mud above 6.35 mcd but increase by up to three orders of magnitude below 6.35 mcd (Figs. 3 and 4). A viscous remanent magnetization (VRM) with anomalous directions is present in all lithologies but can generally be removed with a 10 mT AF demagnetization. Following removal of the VRM, AF demagnetization shows systematic, although sometimes noisy, behavior with magnetic directions demagnetizing towards the origin on a Zijderveld plot (Fig. 3). ARM intensities are stronger but follow the same general pattern as NRM intensities. There are large variations in ferrimagnetic mineral coercivity, tracked by the ratio of the ARM intensity remaining after 20 mT AF demagnetization relative to the primary ARM intensity (ARM_{20mT}/ARM) (e.g. Blanchet et al., 2007; Stoner and St-Onge, 2007), with the lowest coercivity ferrimagnetic mineral assemblages stratigraphically above and below the high density massive gray clay lithologic unit (Fig. 4).

Based on the demagnetization behavior, ChRMs were calculated using a PCA using all values over the 15–50 mT AF demagnetization range without anchoring to the origin. MAD values are higher in the low NRM intensity unit of the upper 6.35 mcd, with the majority ranging from about 5 to 10°. Below, 6.35 mcd, MAD values indicate the ChRM is much better defined, with all values less than 5°. The average ChRM inclination value for all data after removing u-channel edges is 57.1°, similar to the 58° for the site that is predicted based on the assumption of a geocentric axial dipole. 95% of all inclination values are within 16.3° of the average value, consistent with observations of well-defined mid-latitude western North America Holocene paleosecular variation records from archeomagnetic, volcanic, and sedimentary archives (e.g. Hagstrum and Blinman, 2010; Hagstrum and Champion, 2002; Verosub et al., 1986). However, due to the weak NRM intensities in the upper unit, large changes in NRM intensities in the lower unit, and large changes in ferrimagnetic coercivity, we determine this site is not well-suited for a continuous relative paleointensity reconstruction through the entire recovered interval (e.g. Stoner and St-Onge, 2007; Tauxe, 1993), and focus our efforts on the directional PSV record. Future investigations to reconstruct relative paleointensity at Fish Lake, UT may need to consider the lithologic units separately or experiment with objective correction factors (e.g. Brachfeld and Banerjee, 2000; Mazaud, 2006).

To further investigate the directional record from the well-defined ChRM interval below 6.35 mcd, we performed deconvolution experiments on the u-channel data, using UDECON MATLAB tools (Xuan and Oda, 2015) and a conservative smoothness parameter (ln(u)) of 2 in our final result (Fig. 5)). One of the key assumptions required in deconvolution of u-channel data is that the downcore magnetization varies as a smooth function (Jackson et al., 2010). Ultimately, deconvolution models are a trade-off between the model-data misfit, some of which is likely due to measurement error, and smoothness (Jackson et al., 2010; Oda and Shibuya, 1996). Larger, more conservative ln(u) values, similar to the ones employed here, result in a smoother deconvolution solution but are more robust to measurement noise by not allowing solutions that overfit the raw data. As a result, conceptually, our conservative approach to deconvolution may be more akin to

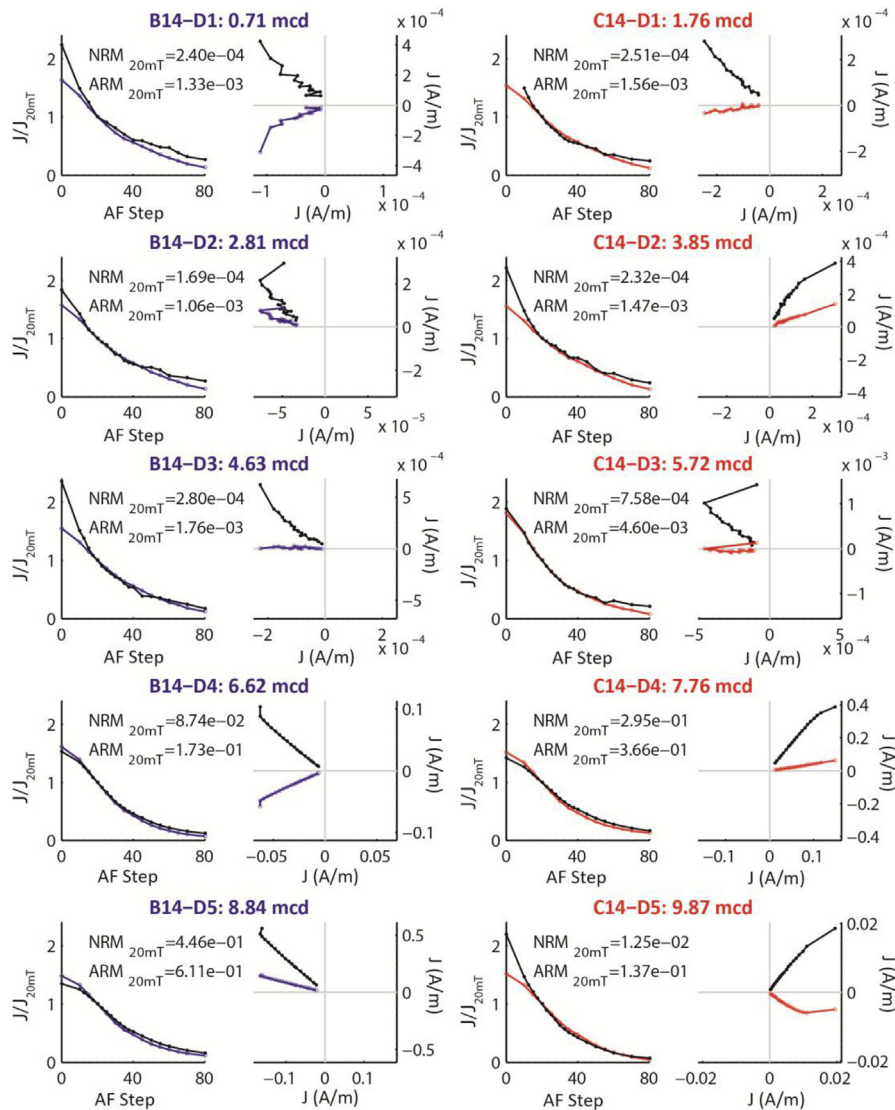


Fig. 3. AF demagnetization behavior of the 25 cm position in each u-channel taken from the Fish Lake, Utah cores. For each pair, (left) magnetization (J) of the NRM (black) and ARM (blue/red) during AF demagnetization normalized by the 20 mT AF demagnetization step and (right) Zijderveld plots (Zijderveld, 1967) of the vertical (black) and horizontal (blue/red) components of the NRM. (For interpretation of the references to color in this figure legend, the reader is referred to the Web version of this article.)

simulating a magnetometer with a narrower response function than solving for discrete 1 cm magnetizations.

To test the results, we compare the deconvolved u-channel SRM data with the u-channel magnetic susceptibility data. The Bartington loop used to collect the magnetic susceptibility data has a narrower response function (~ 3.0 cm FWHM) than the SRM (~ 7.5 cm FWHM). Assuming the concentration of ferrimagnetic minerals is a primary control on both magnetic susceptibility and NRM intensity and that the signals are a reflection of the same geologic processes, we expect the correlation between the two parameters to improve following deconvolution of the NRM, recognizing that in some circumstances magnetic susceptibility and remanence parameters may reflect differences in magnetic mineral assemblages and grain sizes (e.g. Maher, 1988). To test this, we calculate the linear correlation coefficient in 30 cm bins between the detrended logarithmic magnetic susceptibility and detrended logarithmic NRM intensity after 20 mT AF demagnetization (Fig. 5). We use the detrended logarithmic data to mitigate the impact of

large susceptibility and intensity changes and long wavelength variations on the calculation. We find, in most instances, an improvement in correlation coefficients for the deconvolved SRM data. We also note that ChRM MAD values from calculating the PCA of the deconvolved data are not significantly different from those calculated before the deconvolution, suggesting the deconvolution is creating consistent results for each demagnetization step. These findings provide added confidence in our application of the deconvolution method of Oda and Xuan (2014) and in using the deconvolution results in our discussion.

4.2. Stacking paleomagnetic directions for Fish Lake, Utah and Bear Lake, Utah/Idaho

Paleomagnetic data from Fish Lake, UT and Bear Lake were stacked to increase signal to noise and assess uncertainty of the PSV estimates. We do not create a new stack for the Bessette Creek data, but use the data and uncertainty as reported by Turner et al. (1982),

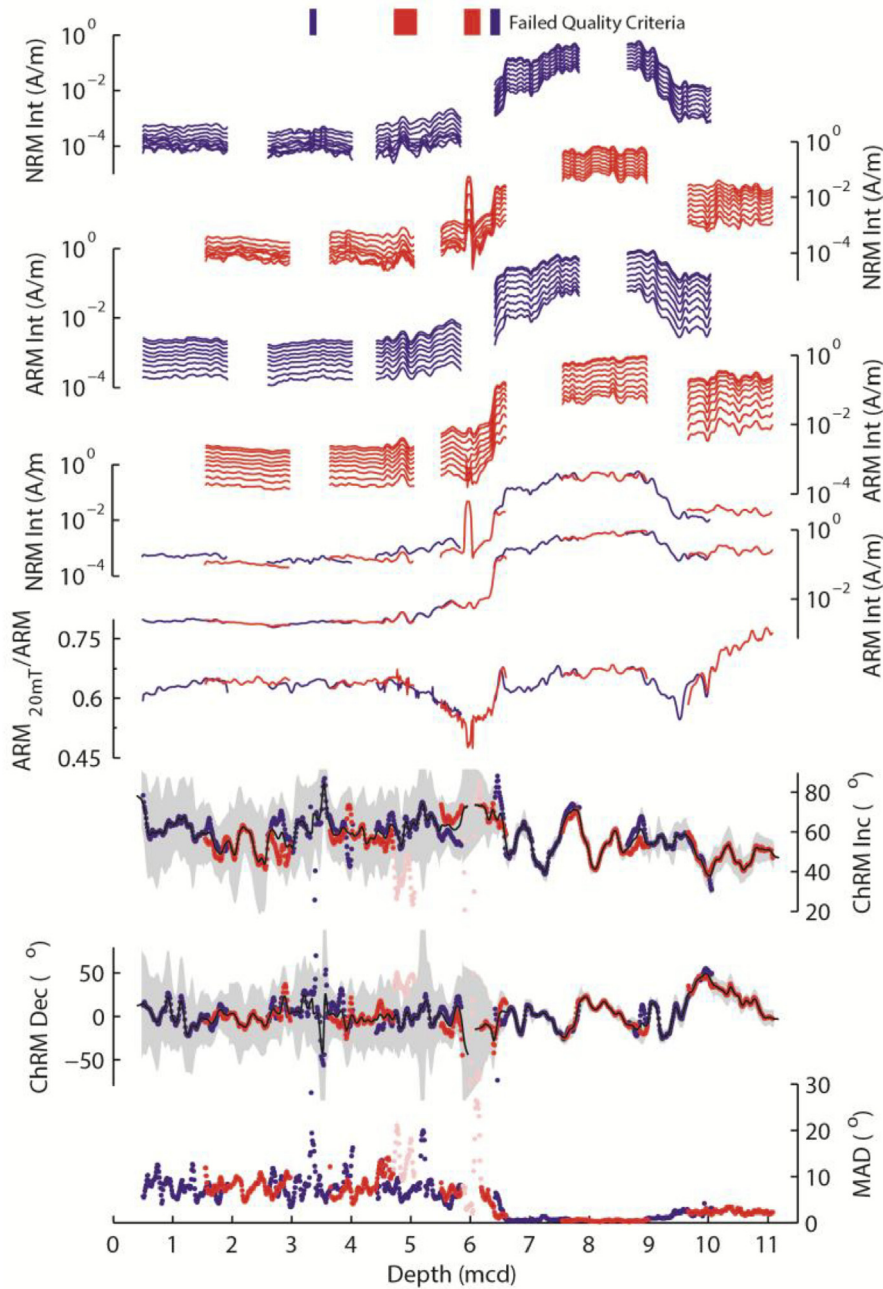


Fig. 4. Magnetic Results for the Fish Lake, Utah cores from holes B14 (blue) and C14 (red). From top to bottom: NRM intensity measured before and after every 10 mT AF demagnetization step between 0 and 80 mT. ARM intensity at the same steps as the NRM intensity. NRM and ARM, before AF demagnetization, plotted as a composite record. ARM coercivity, tracked as the ratio of the ARM after 20 mT AF demagnetization to the ARM before demagnetization. ChRM Inclination and Declination and MAD values are calculated with a PCA for steps measured between 15 and 50 mT AF demagnetization (points). Mean stacked directions are shown (black line) with α_{95} uncertainty (gray shading). Measurements that did not pass quality criteria are plotted in a lighter color. (For interpretation of the references to color in this figure legend, the reader is referred to the Web version of this article.)

as discrete samples were directly sampled from the Bessette Creek outcrop and each stratigraphic horizon is already the mean of 3–4 specimens.

4.2.1. Stacking Fish Lake, Utah cores

Four intervals were not used in the creation of the Fish Lake, UT PSV stack, due to coring disturbances or anomalous magnetic results. High MAD values and negative inclinations in B14-D2 between 3.30 and 3.40 mcd were removed, which most likely result from remagnetization post recovery, although the exact origin is

unknown. Significant gas expansion observed in the CT scans (Fig. 2) at the base of C14-D2 below 4.71 mcd is associated with anomalously shallow inclination values with respect to overlapping sediments in B14-D3 and was also removed. We removed an interval in B14-D4 between 5.86 and 6.17 mcd with anomalously high ARM intensity and low ARM coercivity which also has negative inclinations, suggesting the anomalous magnetic mineralogy is not suitable for paleomagnetic analysis. Finally, we remove the upper 19 cm in the B14-D4 u-channel, above 6.48 mcd, as we suspect the sediments near the top of the core were significantly twisted

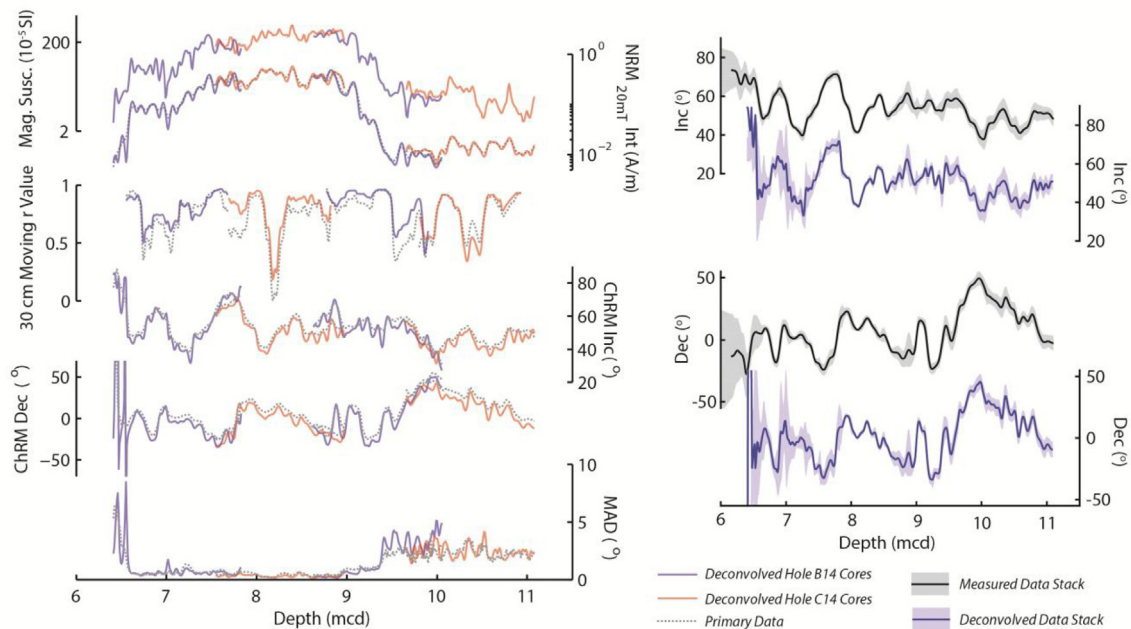


Fig. 5. (Left) Results of deconvolution experiment for the Fish Lake, Utah cores for the 4th and 5th drive from holes B14 (blue) and C14 (red). Primary SRM data are plotted as gray dashed line. From top to bottom: Magnetic susceptibility measured with a 36 mm diameter Bartington loop compared with the NRM intensity after 20 mT AF demagnetization. A 30 cm bin moving correlation coefficient is used to quantify the general improvement in correlation of the detrended logarithmic NRM intensity compared to the detrended logarithmic magnetic susceptibility for each u-channel. ChRM Inclination, Declination and MAD values calculated with a PCA for steps measured between 20 and 50 mT. (Right) Comparison of PSV stacks with 1σ uncertainty made with primary SRM data (black line/gray shading) and deconvolved data (blue line/light blue shading). (For interpretation of the references to color in this figure legend, the reader is referred to the Web version of this article.)

during recovery, leading to a large swing in declination which is not reproduced in C14-D3.

As there was no azimuthal orientation of the cores during recovery, declinations are only relative changes within each core. Accordingly, we first rotated the declination in each core to a mean of zero, calculated after removing edge effects and disturbed intervals. In all but one circumstance, we chose to use this simple correction as it provided a reasonable agreement between overlapping drives. The only exception is for C14-D5. There was a significant offset between B14-D5 and C14-D5 and we added an additional 25° eastward rotation to C14-D5 to account for it.

Our estimates of uncertainty in the stacked Fish Lake, UT PSV record (Fig. 4) suggest that while the low NRM intensity unit at the top of the core is noisy and can only resolve longer wavelength PSV features, the higher NRM intensity unit below 6.35 m has well resolved PSV features. A second stack was created for B14-D4, B14-D5, C14-D4, and C14-D5 using the deconvolution results, with ChRMs calculated in the same manner as the primary data (Fig. 5). The stack created with the deconvolution results does not create any new high amplitude PSV features when compared to the stack created with the primary measured data. The biggest difference is that well-defined PSV features in the deconvolved data stack are more sharply defined.

4.2.2. Stacking Bear Lake, Utah/Idaho cores

The Bear Lake PSV stack was created with all data (Heil et al., 2009) between 9.75 and 25 m from Hole BL00-1D Cores 4H–9H and Hole BL00-1E Cores 4H–9H, after removing u-channel edges and rotating declinations of overlapping sediments to match (Fig. 6). As there is more overlapping sediment between the Bear Lake Cores than the Fish Lake, UT cores, we believe this approach is justified over simply rotating each drive to a mean of zero. However, we found it difficult to rotate Bear Lake declinations with this strategy below 17 m without imparting a large ~ 8 m linear trend to

the east ($\sim 7.5^\circ/\text{m}$). We interpret these linear declination trends to be twisting artefacts of coring. To address this issue, we subtract the linear trends found in BL00-1D Cores 7H and 8H and in BL00-1E Cores 7H–9H. The result improves the agreement in declination in overlapping sediments; however, we recognize that uncertainty in this declination correction could only be fully quantified by more observations from additional overlapping cores. After detrending, the final rotations were $35, 55, -15, 60, 55,$ and -30° for BL00-1D Cores 4H–9H, respectively, and $-50, -40, -30, 90, -10,$ and -125° for BL00-1E Cores 4H–9H, respectively, with positive values indicating eastward rotations.

4.3. Regional comparison and establishing an integrated regional chronology

While we recognize broadly consistent PSV signals between the three sites for the Late Pleistocene, we also know that all three sites, like many Late Pleistocene records, do not have the strong independent chronologies needed to make robust comparisons of these features on age. Accordingly, we adopt the approach of Stoner et al. (2007) by correlating the Fish Lake, UT (deconvolved), Bear Lake, and Bessette Creek records to a common depth scale through graphical correlation and transferring available age control points to a single age-depth model (Table 4; Fig. 7). We choose the Bear Lake BL00 depth scale as the common depth scale, as the Bear Lake record spans the longest period of time. To account for any geometric effects due to variations in latitude and longitude between the three sites, directions were projected to Seattle, Washington ($47.621^\circ\text{N}, 122.349^\circ\text{W}$) via their virtual geomagnetic pole (VGP) paths. This site was chosen as it is a mid-latitude location for Western North America and will establish a central location for future work that will explore high resolution Northeast Pacific marine and Western North American terrestrial archives. While we find good agreement between the absolute projected inclinations

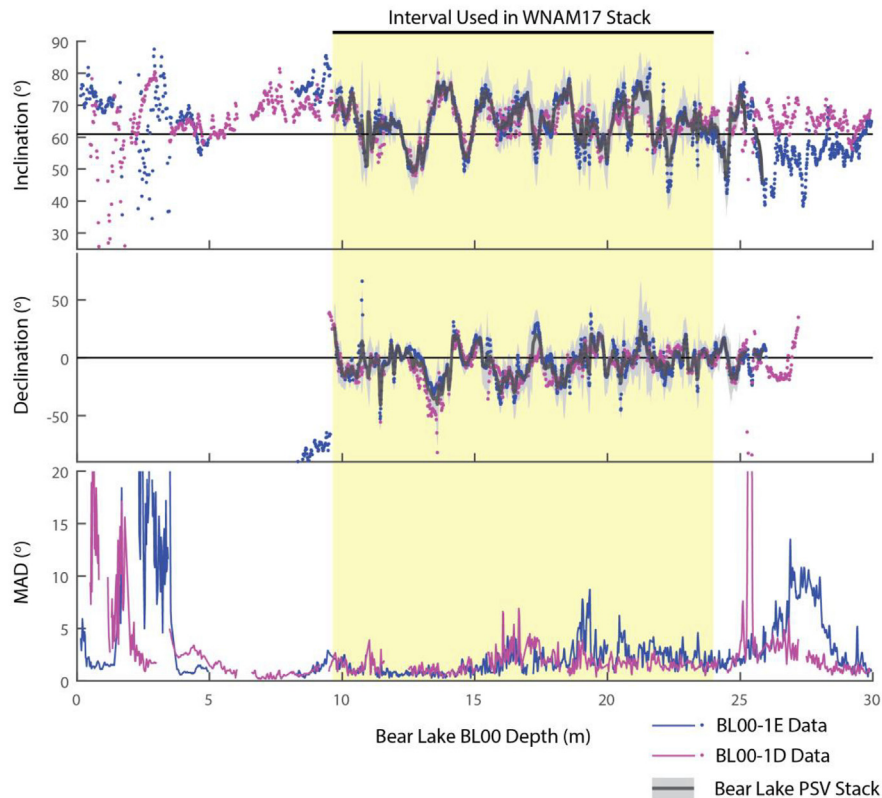


Fig. 6. Paleomagnetic data from Bear Lake Drill Holes BL00-1D and BL00-1E (Heil et al., 2009). All inclination data are plotted, but only corrected declination data from cores used in the stack as discussed in the text. While data were stacked from 9.7 to 25 m, only the 9.7–24 m data (yellow shading) were used in the WNAM17 PSV stack, as this was the interval that overlapped with the Fish Lake, UT and Bessette Creek, BC records. Horizontal black lines indicated the predicted values based on the geocentric axial dipole hypothesis for the Bear Lake latitude. (For interpretation of the references to color in this figure legend, the reader is referred to the Web version of this article.)

Table 4

Tie points to regional depth scale.

Fish Lake, UT		Bessette Creek, BC	
Fish Lake, UT Depth (mcd)	Bear Lake BL00 Depth (m)	Bessette Creek Elevation (m)	Bear Lake BL00 Depth (m)
0	0	14.45	17.15
6.4	9.7	8.2	19.04
6.56	10.8	6.93	20.19
6.77	11.18	4.07	21.28
7.01	12.32	2.11	22.65
7.42	13.15		
7.77	14.09		
7.87	14.29		
8.01	14.46		
8.25	15.15		
8.42	15.42		
8.85	16.98		
9.16	17.53		
9.67	18.66		
10.85	20.25		

in Fish Lake, UT and Bessette Creek, Bear Lake inclinations are on average about 8° steeper. This difference could be the result of coring artefacts (e.g. drilling overprint or minor deformation) or poorly understood differences in sediment magnetic remanence acquisition that might result from differences in each basin's depositional processes. Since we are primarily interested in relative PSV variations for stratigraphic purposes, we subtract 8° from Bear Lake inclinations for the regional stack, as Fish Lake, UT and Bessette Creek agree and Bear Lake site inclination values are almost always greater than predicted based on the geocentric axial dipole

hypothesis (Fig. 7a). However, additional paleomagnetic observations are needed to fully assess the inclination differences. Declination from all three records agree well and we do not apply any further correction. We consider these reasonable estimates for past absolute changes in declination, as the Bessette Creek data are derived from oriented outcrop samples and the furthest distance (~ 1500 km) between two sites is about half the distance associated with spherical harmonic degree 6–7 wavelengths, which is used as the distance for relative declination orientation in the pfm9k spherical harmonic model (Nilsson et al., 2014). Stacking the three

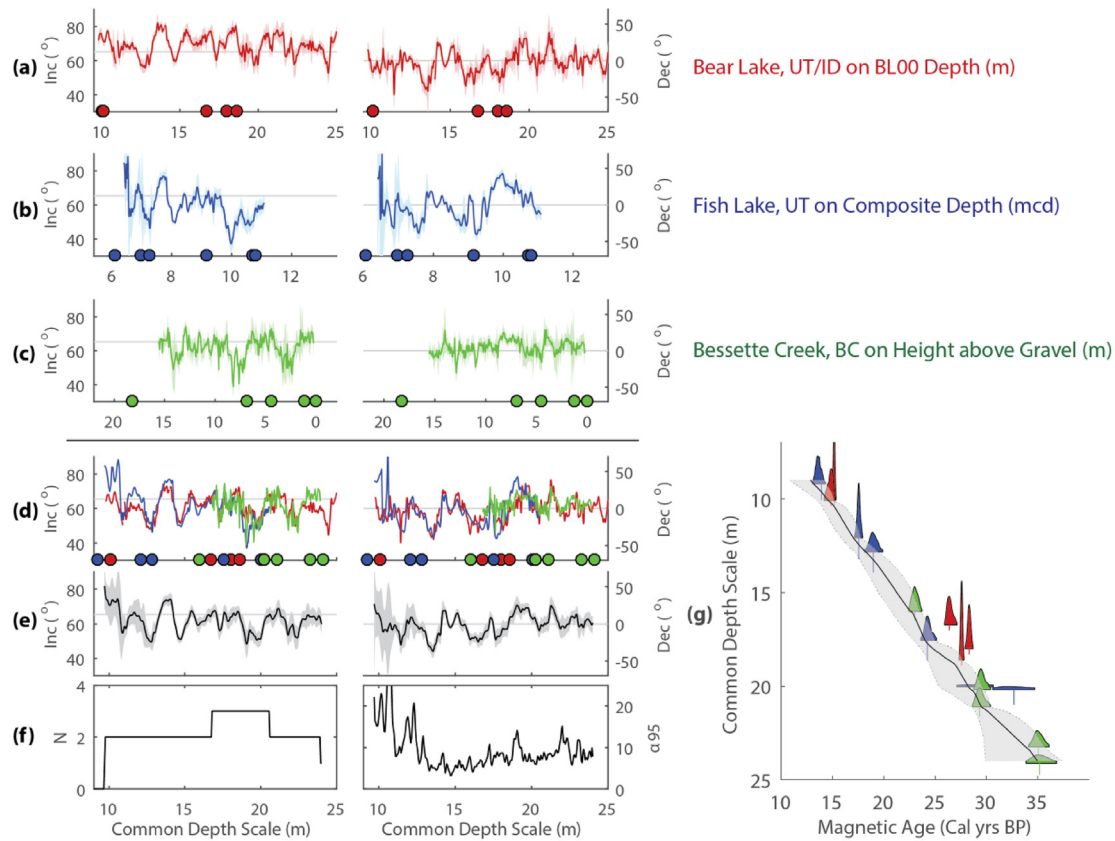


Fig. 7. PSV records, projected to Seattle, Washington via their VGP paths, with 1 sigma uncertainty and age control points for Bear Lake (red, **(a)**), Fish Lake (blue, **(b)**), and Bessette Creek (green, **(c)**). Correlated PSV records **(d)** were used to create the WNAM17 PSV Stack **(e)**, which averages 2–3 records and typically has α_{95} uncertainty of less than 10° **(f)**. Horizontal gray lines in **(a)–(e)** reflect predicted inclination and declination values based on the geocentric axial dipole hypothesis for the latitude of Seattle. **(g)** ^{14}C age estimates, transferred to the common depth scale, were calibrated to calendar years and the median and 95% confidence interval age-depth model for the WNAM17 PSV stack was generated from 10,000 accepted model runs, as described in the text. Calibrated age PDFs from each site are indicated with colors matching **(a)–(c)** and the transferred maximum range for lock-in offset (30 cm) is indicated by a vertical line. The regional chronostratigraphic model factors three main sources of uncertainty: (1) the measurement precision and calibration of the radiocarbon measurements, (2) that only a subset of age estimates closely approximate the age of the sediment, and (3) that there is an unknown difference in the age of the sediment and the age of the magnetization. (For interpretation of the references to color in this figure legend, the reader is referred to the Web version of this article.)

records, using the same method as described above, reveals a well resolved regional signal with α_{95} values typically less than 10° , which we have named the WNAM17 (Western North American 2017) PSV stack (Fig. 7e–f).

The resulting age-depth relationship of the three integrated records contains a number of age reversals, notably the pollen extract radiocarbon ages between 16 and 19 m in Bear Lake, the peat radiocarbon ages from Bessette Creek, and a small mass (0.04 mg carbon) sample with large uncertainty from Fish Lake, UT. While this could result from mismatches in the PSV correlations, some age reversals are not surprising given the difficulty in dating Late Pleistocene terrestrial archives devoid of high quality macrofossils and, in the case of Bessette Creek, limitations in samples appropriate for radiocarbon dating before the advent of accelerated mass spectrometry (Westgate and Fulton, 1975). While post-glacial Bear Lake pollen extract samples generally give younger ages by several hundred years than paired total organic carbon (TOC) and/or carbonate samples, suggesting less contamination from old carbon (Colman et al., 2006), Colman et al. (2009) found last glacial pollen extract ages were up to several thousand years older than stratigraphically lower samples and attributed this difference to higher relative proportions of refractory organic carbon in the extracts. As a result, the authors rejected many of these dates from their age model. The three pollen extracts used in their age model and this study from below the facies interpreted as the local glacial

maximum were described as containing better preserved pollen. Similarly, the rest of our age control points, particularly the peat samples, are all samples that could have issues with being anomalously old and incorporating reworked carbon from the landscape. Few samples, if any, used in the creation of the WNAM17 age model are the high quality terrestrial macrofossils needed to closely approximate the age of the sediment, such as deciduous leaf macrofossils (e.g. Howarth et al., 2013). Nevertheless, these terrestrial samples have little risk for modern carbon contamination, as has been demonstrated to impact some lake carbonate samples from Western North America by progressive leaching (Hajdas et al., 2004; Kent et al., 2002), or complications from old lake carbon reservoir issues. At a minimum, these ages can be considered robust maximum limiting ages.

Another source of age uncertainty for the WNAM17 PSV Stack is that the age of the physical sediment and age of the sediment magnetization are not necessarily equal due to sediment magnetization acquisition in a lock-in zone following deposition (e.g. Egli and Zhao, 2015; Irving and Major, 1964; Løvlie, 1976; Verosub, 1977). While sediment magnetization acquisition processes are not completely understood and may result from different processes in different depositional environments, studies commonly find decimeter offsets in the age of magnetizations in bioturbated and varved sediments where independent chronometers and/or superposition allow comparison (Channell and Guyodo, 2004;

deMenocal et al., 1990; Mellström et al., 2015; Nilsson et al., 2018; Simon et al., 2018; Snowball et al., 2013; Stoner et al., 2013; Suganuma et al., 2010).

Given these known uncertainties, we use an age-depth modeling approach inspired by Haslett and Parnell (2008) to calculate an ensemble of possible age depth combinations that capture the uncertainty structure of the WNAM17 age of magnetization—particularly uncertainty related to (1) radiocarbon data precision and calibration; (2) reworking of old carbon; and (3) depth offsets in the magnetization age. Assuming that all age control points are robust maximum limiting ages but only a subset approximate the actual age of the sediment, we start each iteration by randomly selecting eight of the sixteen (50%) age control points. The ages of the control points are then randomly selected from the calibrated age probability distribution function (PDF) and the depth from a uniform distribution ranging from 0 cm (no offset in magnetization age) to 30 cm (large offset in magnetization age) and then transferred to the common BLOO Bear Lake depth scale. We believe this range is justified; while some studies argue for little or no offset (Valet et al., 2014), many observations suggest offsets of up to 14–25 cm (Channell and Guyodo, 2004; Simon et al., 2018; Stoner et al., 2013; Suganuma et al., 2010) or more in some cases (Snowball et al., 2013). Additional synthetic age-depth pairs are then added at random between these age control points to allow for non-linear accumulation rates between dated horizons. While the spacing of synthetic age-depth pairs varies for each iteration, the result is approximately four real and/or synthetic age-depth pairs per meter. We reject the iteration if there are age reversals, as this violates the law of superposition, or if any of the sixteen dated horizons are older than its maximum limiting radiocarbon constraint, defined as the 99th percentile of the calibrated PDF. The model is run until 10,000 iterations are accepted. The result is an age-depth relationship for the magnetization age of the WNAM17 PSV Stack with large, but realistic uncertainty (median 95% confidence interval of ~1.5 ka), allowing for refinement with future work (Fig. 7). The greatest strength of our age-depth model is that by approaching chronostratigraphy from a regional perspective, assuming a common geomagnetic signal, we can address sources of geologic uncertainty that would be difficult to quantify using only one site.

5. Discussion

5.1. Implications for regional chronologies and the timing of major lithologic transitions

Development of the independently dated WNAM17 PSV stack provides a template for improving or assessing regional chronologies. As a first exercise, we look at the impact on the timing of major lithologic changes observed at Fish Lake, UT and Bear Lake, UT/ID on their independent chronologies and WNAM17 'tuned' chronologies. We use the original correlations defined between Fish Lake, UT and Bear Lake that were used when building the stack and compare those depths to the ages of the same integrated horizons in the WNAM17 Stack (Table 4). This ensures each record has the same number of correlation points and each correlation point is at a PSV feature that was recognized at both Fish Lake, UT and Bear Lake, UT/ID. We generate PDFs from the ensemble of age-depth models discussed in Section 3.3 at each tie point, which then can be used to create a new ensemble of site age-depth models.

Age-depth modeling is done as in Section 3.3, with a few modifications (Fig. 8). First, we do not need to drop any age control points, as all dates based from the WNAM17 template are in stratigraphic order and are estimates for the sediment's age of magnetization. Second, we do not need to use the maximum

limiting age constraint for the same reason. Third, we do not perturb the depths of the age control points; rather, we run two simulations to illustrate the potential influence of constant offsets in magnetization age—with one assuming no offset (no pDRM) and the other assuming a constant 15 cm offset (pDRM offset like documented elsewhere). While it may be simpler for these two lakes to just take the WNAM17 age-distributions at horizons of interest, we create new age models in this way to illustrate how the WNAM17 stack could be used with other records where age-control points can only be defined by where there are strong PSV correlations. To illustrate the chronologic implications, we also use the published age-depth model of Colman et al. (2009) for Bear Lake, and a new age-model for Fish Lake, UT, using only the Fish Lake, UT radiocarbon and tephra age control points, generated in the same fashion as the WNAM17 tuned chronologies.

We treat major lithologic transitions as events and generate PDFs of the event age from each of the age models described above (Fig. 8c). For Bear Lake, the transitions are defined as the increase in magnetic susceptibility below the red siliciclastic unit (18 m) and the top of the red siliciclastic unit (10.4 m), interpreted as being deposited during the local glacial maxima (Colman et al., 2009; Heil et al., 2009; Kaufman et al., 2009; Rosenbaum and Heil, 2009). For Fish Lake, UT, the transitions are defined by the bottom (9.17 m) and top (6.41 m) of the high-density and high magnetic susceptibility unit (Fig. 2). The focus here is to discuss the timing of the changes. A detailed study of the paleoenvironmental and glacial implications of these records will be discussed elsewhere.

On each site's independent chronology, the base of the lithologic transitions would be considered separate events, with the transition at Bear Lake preceding the transition at Fish Lake, UT (Fig. 8c). Applying the WNAM17 tuned chronology pushes the onset of this event much younger at Bear Lake (~24–26 ka), with the new PDF overlapping with that found at Fish Lake, UT independently of the depth in magnetization offset we use. Similarly, for the top of the lithologic unit, while the age of the transition is poorly defined at Fish Lake, UT on its independent chronology, applying the WNAM17 tuned chronology provides a stronger constraint for its age (~14–16 ka). In both cases, a slightly better agreement can be generated by invoking magnetic lock-in offsets, that vary in time depending on sedimentation rate.

While there is no direct evidence that indicates that these lithologic changes need to be regionally consistent, we consider this anecdotal support for application of the WNAM17 template to problems such as the timing of geologic events. Within the context of regional PSV stratigraphy and uncertainties in radiocarbon dating and the magnetic acquisition processes, we cannot rule out the possibility that major glacial changes in the Late Pleistocene occurred in phase in these two basins.

5.2. Assessing the chronology of Mono Lake, California

In our second exercise, we apply the WNAM17 PSV stack as a reference to the magnetic record at Mono Lake, California. While, many are interested in the age of the geomagnetic excursion found at this site, our goal in this discussion is not to give a definitive answer, but to explore the PSV stratigraphic context of the event and discuss the implications for proposed timings of that event.

The chronology of sediment outcrops at Mono Lake have received considerable attention for resolving the age and uniqueness of the geomagnetic excursion recorded in its sediments (Benson et al., 2003a; Cassata et al., 2010; Kent et al., 2002; Lund et al., 2017; Vazquez and Lidzbarski, 2012; Zimmerman et al., 2006) and the relationship between paleoenvironmental signals and abrupt climate and/or orbital climate signals (Benson et al., 2003b, 1998; Zimmerman et al., 2011a, 2011b). Initial

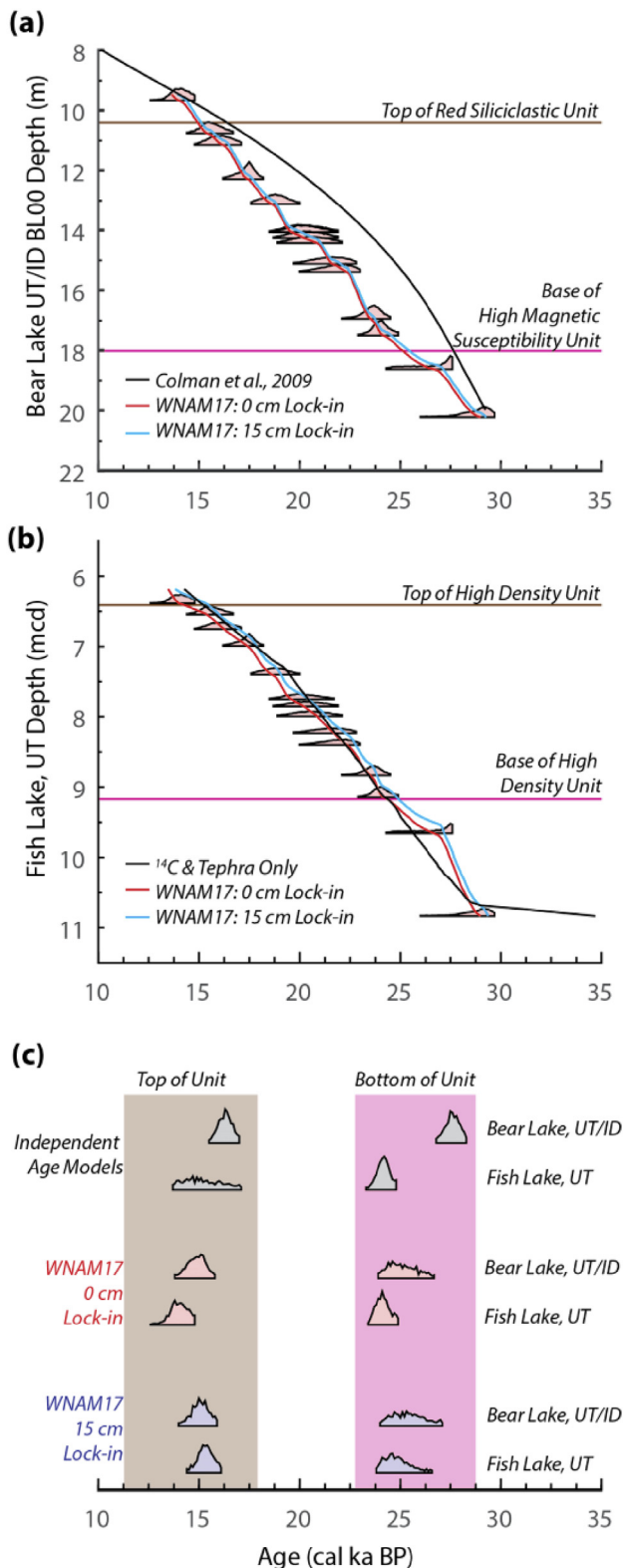


Fig. 8. Comparison of the ages of major lithologic contacts observed at Bear Lake, UT/ID and Fish Lake, UT. Age depth models for (a) Bear Lake, UT/ID and (b) Fish Lake, UT were generated using WNAM17 age PDFs (light red shading) at PSV correlation horizons (Table 4). Two age models were generated to illustrate age-depth relationships if sediment and magnetization ages are equal (0 cm lock-in; median age = red line) or if the age of the magnetization is offset by 15 cm (15 cm lock-in; median age = light blue line). For comparison, the previously published Bear Lake age model (Colman et al., 2009) and an age model generated only using age control points from Fish Lake, UT are plotted (black lines). (c) The resulting age PDFs for the two lithologic contacts for

paleomagnetic work recognized a high-amplitude declination feature around ash layer 15 in the Wilson Creek Formation (Denham and Cox, 1971), which was later defined with more detailed work as a significant and reproducible geomagnetic excursion recorded at Mono Lake (Liddicoat and Coe, 1979). Lund et al. (1988) compiled previously published and new PSV data for the Wilson Creek Formation, revealing a well-resolved and high-amplitude record of Late Pleistocene PSV and placed the excursion event in the context of longer term geomagnetic change. As there is no community consensus on the chronology of the Wilson Creek Formation at Mono Lake, the WNAM17 PSV stack provides the opportunity to assess the Wilson Creek Formation chronology where they overlap in time.

While the initial chronology for the complete record was constrained by radiocarbon dating of carbonate samples, including tufa and ostracods (Benson et al., 1990; Lund et al., 1988), progressive leaching of radiocarbon samples indicated significant contamination by young carbon, suggesting age estimates for these sediments were too young and radiocarbon dates may only represent a minimum limiting age (Hajdas et al., 2004; Kent et al., 2002), which seems to support older radiometric dates on ash layers surrounding the excursion (Cassata et al., 2010; Cox et al., 2012; Kent et al., 2002; Vazquez and Lidzbarski, 2012; Zimmerman et al., 2006). However, the radiocarbon ages are also complicated by unknown changes in potentially very large reservoir ages (on the order of 10^3 yrs; Benson et al., 1990; Broecker et al., 1988) and radiometric dating of ash layers have been argued as being only maximum limiting ages and not direct dates of the eruptions (e.g. Cassata et al., 2010; Kent et al., 2002; Negrini et al., 2014), requiring assessment by independent stratigraphic correlation.

Independent stratigraphic correlation has previously been attempted using tephra and paleomagnetic correlation. For example, Benson et al. (2003a) identified a tephra layer with similar chemical composition to the Wilson Creek Formation ash layer 15, which transects the excursion, in the Pyramid Lake Basin, Nevada with a ¹⁴C age of $28,620 \pm 300$ yrs (IntCal13 2 σ : 31,693–33,474 cal yrs BP with no reservoir correction) based on total organic carbon, which may be impacted by reservoir ages (estimated at ~600 yrs in the late Holocene), but should not face the same young carbon contamination as the carbonate samples in Mono Lake. Excursion directions have also been documented just beneath this ash layer in sediment cores from Pyramid Lake (Lund et al., 2017) and outcrops within the basin (Liddicoat, 1992). Conversely, a paleomagnetic correlation, based on relative paleointensity, supports an older age for the excursion at Mono Lake, coeval with the age of the Laschamp Excursion documented elsewhere (Zimmerman et al., 2006) with an age of ~41 ka (Laj et al., 2014; Lascu et al., 2016; Nowaczyk et al., 2012). While this chronology is consistent with ²³⁸U–²³⁰Th ages of the most recent crystallization of allanite crystals at multiple ash layers (Vazquez and Lidzbarski, 2012), it is difficult to reconcile with the leached carbonate radiocarbon samples (Cassata et al., 2010). Less visually appealing correlation scenarios than the Zimmerman et al. (2006) relative paleointensity correlation proposed by Cassata et al. (2010) could easily be justified as reflecting variations in magnetic remanence acquisition efficiency in different Wilson Creek Formation lithologic units, as the intervals with highest absolute values of normalized NRM intensity (the relative paleointensity proxy) are consistently found in lithologic units with the lowest weight percent total inorganic carbon (e.g. Benson et al., 1998).

Our WNAM17 PSV Stack offers an independent opportunity for

each set of age models. (For interpretation of the references to color in this figure legend, the reader is referred to the Web version of this article.)

stratigraphic correlation, using the well resolved PSV record of Lund et al. (1988) and transferred to the Wilson Creek Formation type section height by linear interpolation between ash layers. While PSV correlation to distal Western North Atlantic Sites has been conducted previously (Benson et al., 1998; Lund et al., 2017), we feel our approach is simpler and requires fewer assumptions about the synchronicity of inclination and declination features over significantly larger length scales. For direct comparison with the WNAM17 PSV Stack, the Mono Lake directions are also projected to Seattle, Washington via their VGP path. For the purposes of this discussion we do not apply an offset to the magnetization, as we are comparing a magnetic age at Mono Lake to magnetic age in the WNAM17 template. We feel this is appropriate, but it is important to note that when comparing to the radiocarbon and ash layer dates our magnetic ages may indicate a slightly older age for the sediment, with age offsets depending on accumulation rates.

Correlation of PSV features is straight forward for sediments from the top of the section to just below ash layer 7, with good agreement in inclination and declination without invoking large sedimentation rate changes. These PSV features are also in good agreement with the available radiocarbon samples, given their uncertainty, and the Vazquez and Lidzbarski (2012) ^{238}U – ^{230}Th date of ash layer 7, giving us confidence in this approach and adding significantly stronger chronologic constraint to these sediments than previously available. Differences in $^{40}\text{Ar}/^{39}\text{Ar}$, ^{238}U – ^{230}Th , and ^{14}C age estimates become more pronounced below this level.

Moving down section, below ash layer 7, the Mono Lake PSV record has a number of high amplitude PSV features. The excursion occurs during a longer wavelength inclination steepening, overlain by a broad interval of shallower inclinations. The excursions feature also occurs during a longer wavelength period of eastern declinations, overlain by a broad interval of western declinations.

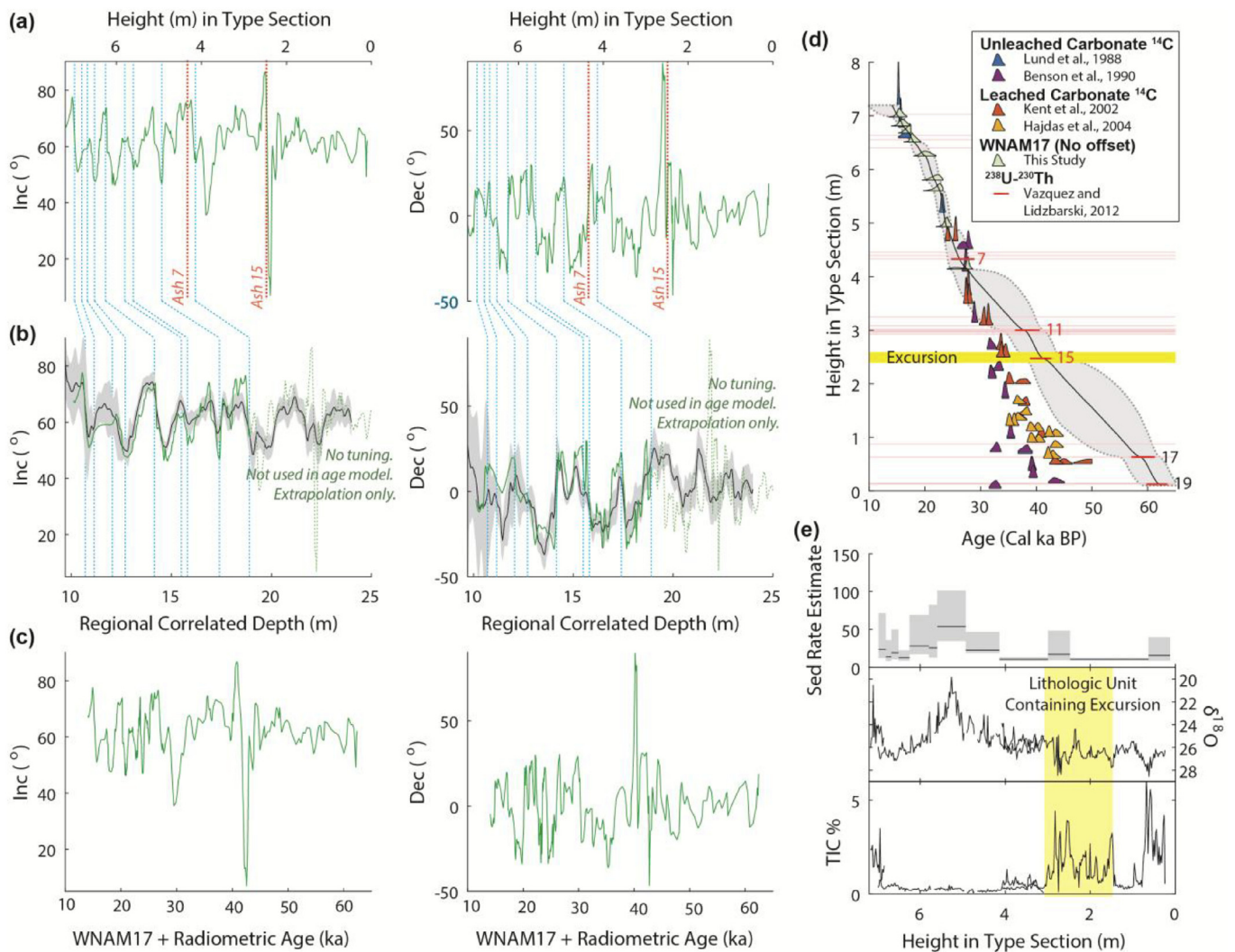


Fig. 9. PSV Tuning exercise comparing the Mono Lake PSV record to the WNAM17 PSV Stack, following Scenario 1 in the main text (Section 3.5.2.1). (a) PSV record from Mono Lake (green line; Lund et al., 1988) transferred to the type section height by linear interpolation between ash layers. Vertical lines indicate the positions of Ash Layers 7 and 15. (b) Correlation of the Mono Lake PSV record to the WNAM17 PSV Stack (black line with 1σ uncertainty displayed in gray shading). Light blue lines are used to display tie points. In this scenario, PSV correlation is only used where there is good agreement between all chronometers to just below Ash Layer 7. (c) The resulting PSV record on age, using the age depth model in (d). (d) Probability distribution functions (PDF) of the ages of tie points to the WNAM17 PSV Stack (light green) and ^{238}U – ^{230}Th radiometric constraints on Ash Layers 11–19 from Vazquez and Lidzbarski (2012) where used to develop 10,000 age models with median (black line) and 95% confidence interval (gray shading). This age model is compared to radiocarbon estimates from leached (Hajdas et al., 2004; Kent et al., 2002) and unleached (Benson et al., 1990; Lund et al., 1988) carbonate samples. Ash layers (pink) and the excursion, defined by the interval including the eastern most declination swing and shallowest inclination, (yellow) are included for reference. (e) Resulting sedimentation rates with 1σ uncertainty calculated from the linear sedimentation rates between tie points, compared with lithologic and paleolimnology proxies of Benson et al. (1998). (For interpretation of the references to color in this figure legend, the reader is referred to the Web version of this article.)

This pattern is typical of what is described for other examples interpreted as the Mono Lake Excursion at other locations in Western North America (Negri et al., 2014, 1984). However, we note that while the immediately older PSV pattern in the WNAM17 PSV Stack fits this description, there is no excursions behavior documented in this depth interval at any of our sites. Thus, there are at least two alternatives. As almost any stratigraphic correlation is non-unique, we present a case for each scenario with their respective magnetic, chronologic, and sedimentological implications. In each case, the PSV tie points from the top of the section to just below ash layer 7 are the same.

5.2.1. Scenario 1: the Laschamp Excursion recorded at Mono Lake

Reconciling the strong PSV based chronology above ash layer 7

and the ^{238}U – ^{230}Th allanite dates below requires a decrease in sedimentation rates, relative to the overlying sediments, or a hiatus in sedimentation between ash layers 7 and 11 (Fig. 9). We have difficulty finding a strong agreement in both inclination and declination consistent with a lower sedimentation rate scenario that still has good visual correlation with inclination and declination. Notably, the broad eastward declination and broad shallow inclination features centered around 4 m elevation in the Wilson Creek Formation type section, would need to be stretched to encompass two large eastward declination and two shallow inclination features between about 18 and 23 m in the WNAM17 PSV Stack. This could be the result of low and/or variable sedimentation rates attenuating or distorting the PSV signal (e.g. Balbas et al., 2018; Lund and Keigwin, 1994; Valet and Fournier, 2016). It is

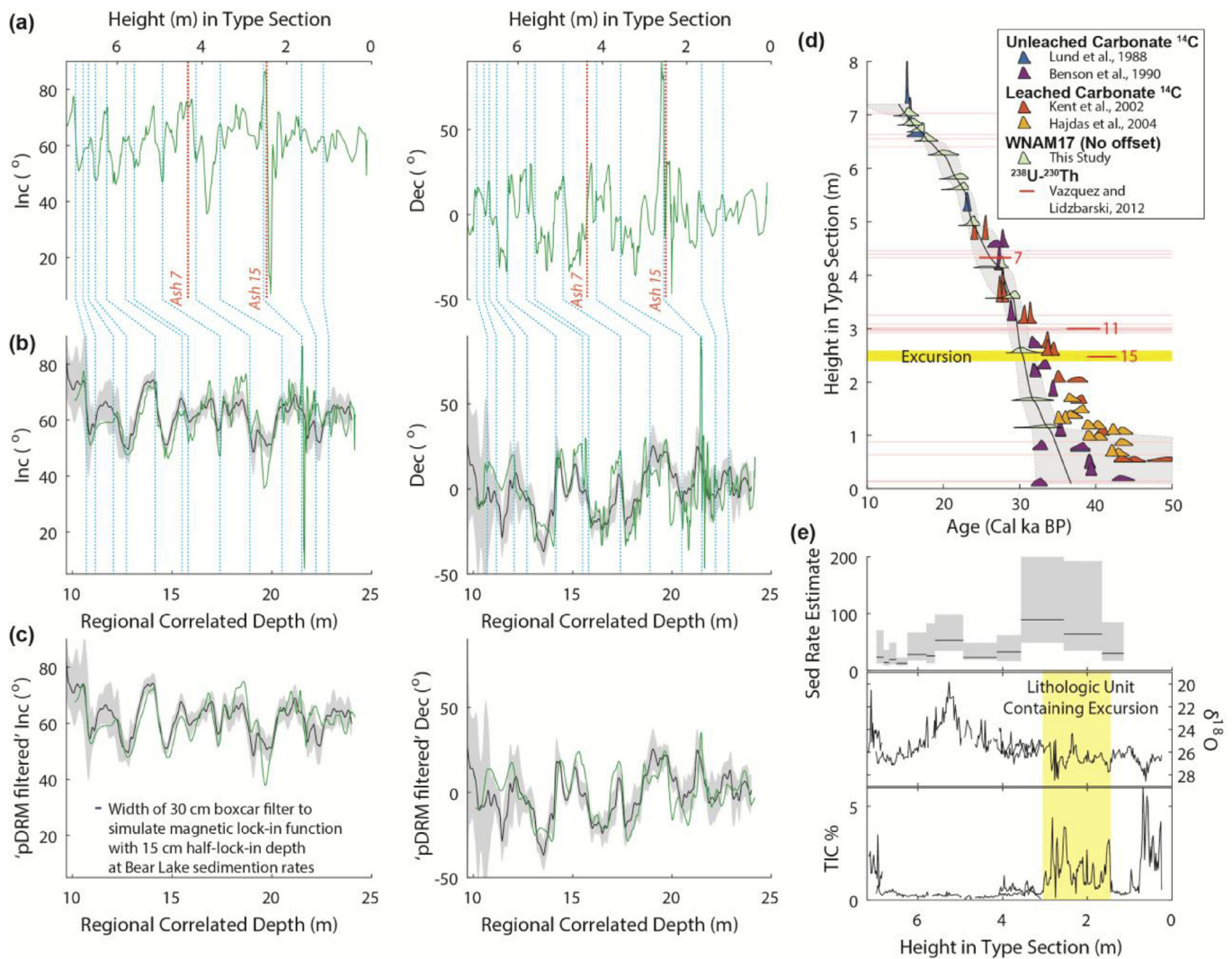


Fig. 10. PSV Tuning exercise comparing the Mono Lake PSV record to the WNAM17 PSV Stack, following Scenario 2 in the main text (Section 3.5.2.2). (a) PSV record from Mono Lake (green line; Lund et al., 1988) transferred to the type section height by linear interpolation between ash layers. Vertical lines indicate the positions of Ash Layers 7 and 15 (b) Correlation of the Mono Lake PSV record to the WNAM17 PSV Stack (black line with 1σ uncertainty displayed in gray shading). Light blue lines are used to display tie points. (c) The result of applying a simple 15 cm half lock-in linear pDRM model (i.e. 30 cm boxcar filter) to the correlated Mono Lake PSV record on the regional correlated depth scale of WNAM17, illustrating that the excursion at Mono Lake may not be recorded in all sedimentary archives from the region due to smoothing (e.g. Channell, 2017). (d) Probability distribution functions (PDF) of the ages of tie points to the WNAM17 PSV Stack (light green) were used to generate 10,000 age models with median (black line) and 95% confidence interval (gray shading). This age model is compared to radiocarbon estimates from leached (Hajdas et al., 2004; Kent et al., 2002) and unleached (Benson et al., 1990; Lund et al., 1988) carbonate samples. ^{238}U – ^{230}Th dating of allanite rims at Ash Layer 7, 11, and 15 (Vazquez and Lidzbarski, 2012), which are in good agreement with the relative paleointensity based chronology of Zimmerman et al. (2006), are also shown. Ash layers (pink) and the excursion, defined by the interval including the eastern most declination swing and shallowest inclination, (yellow) are included for reference. (e) Resulting sedimentation rates with 1σ uncertainty, calculated as the linear accumulation rates between correlation points, compared with lithologic and paleolimnology proxies of Benson et al. (1998). (For interpretation of the references to color in this figure legend, the reader is referred to the Web version of this article.)

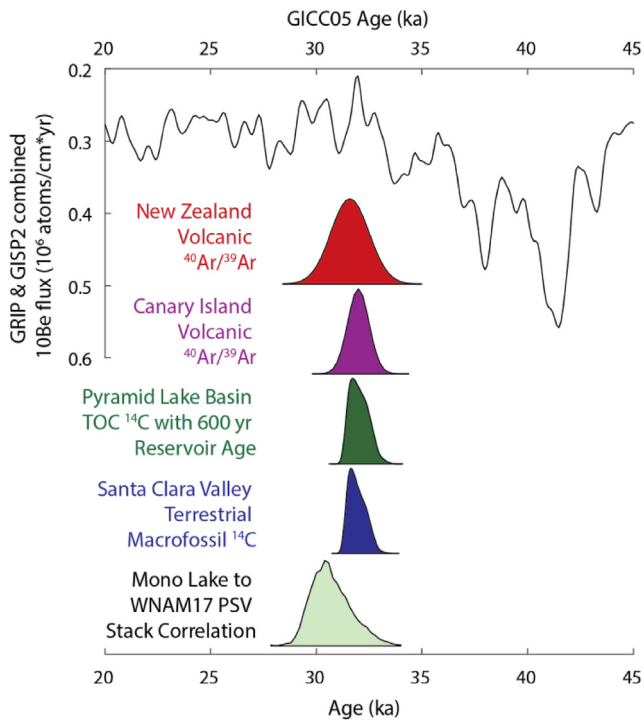


Fig. 11. Comparison of our WNAM17 PSV Stack Scenario 2 correlated age of the excursion at Mono Lake to independent radiocarbon estimates from other regional records (Benson et al., 2003a; Mankinen and Wentworth, 2004), $^{40}\text{Ar}/^{39}\text{Ar}$ estimates from global volcanic records (Cassata et al., 2008; Kissel et al., 2011), and the ^{10}Be flux in Greenland Ice Cores (Muscheler et al., 2014), smoothed using a 392 year FWHM Gaussian Filter. All radiocarbon estimates are calibrated to the IntCal13 timescale and $^{39}\text{Ar}/^{40}\text{Ar}$ are calibrated following the recommendation of Singer (2014). While these age estimates are all within uncertainty of each other, an age-depth model that gives an older age for the excursion recorded at Mono Lake, Scenario 1 displayed in Fig. 9c gives an age for the excursion that is consistent with the high ^{10}Be flux around 41 ka associated with the globally recognized Laschamp excursion.

also possible that there is an unrecognized hiatus.

As we don't have PSV based age control beyond the constraints of our stack, for this exercise we combine our tie points with age control points from the ^{238}U – ^{230}Th allanite dates at ash layers 11, 15, 17, and 19 (Fig. 9) (Vazquez and Lidzbarski, 2012), as these age control points are in good agreement with the relative paleointensity age model of Zimmerman et al. (2006), used to support the interpretation that they are good estimates of eruption age. The results of 10,000 age model realizations suggest relatively low long-term sedimentation rates (on the order of 10 cm/ka) for the sediments deposited below about 4 m, although variations in sedimentation rate cannot be assessed.

5.2.2. Scenario 2: the excursion at Mono Lake occurred between 30 and 34 cal ka BP

In our second scenario (Fig. 10), we continue tuning the PSV record below Ash Layer 7 to the extent of the WNAM17 template. Sedimentation rates are roughly comparable between ash layers 7 and 11 to the sediments overlying ash layer 7 and increase below ash layer 11 (Fig. 10). In this scenario, ^{238}U – ^{230}Th allanite dates would be anomalously old, meaning the final stages of allanite crystallization are not equivalent to the eruption ages, and Cox et al.'s (2012) (U–Th)/He ages of ash layer 15 would need to reflect multiple populations of ages, with only the youngest population (i.e. 34.9 ± 1.1 ka; 35.2 ± 1.1 ka) approaching the true eruption age (e.g. Negrini et al., 2014). The resulting excursion recorded at Mono Lake would be a short event (on the order of 10^2 yrs), meaning Bear Lake and Bessette Creek records do not preserve the excursion because of signal attenuation related to differences in depositional processes, sedimentation rates, and their impact on magnetic acquisition (Balbas et al., 2018; Lund and Keigwin, 1994; Valet and Fournier, 2016). This is a common phenomenon, with geomagnetic excursions often recorded in some sedimentary archives and not others from the same region (e.g. Channell, 2017). To illustrate this point, we use a simple linear pDRM model with half lock-in depth of 15 cm (i.e. a 30 cm wide boxcar filter) on our PSV correlation depth scale (i.e. the depth scale

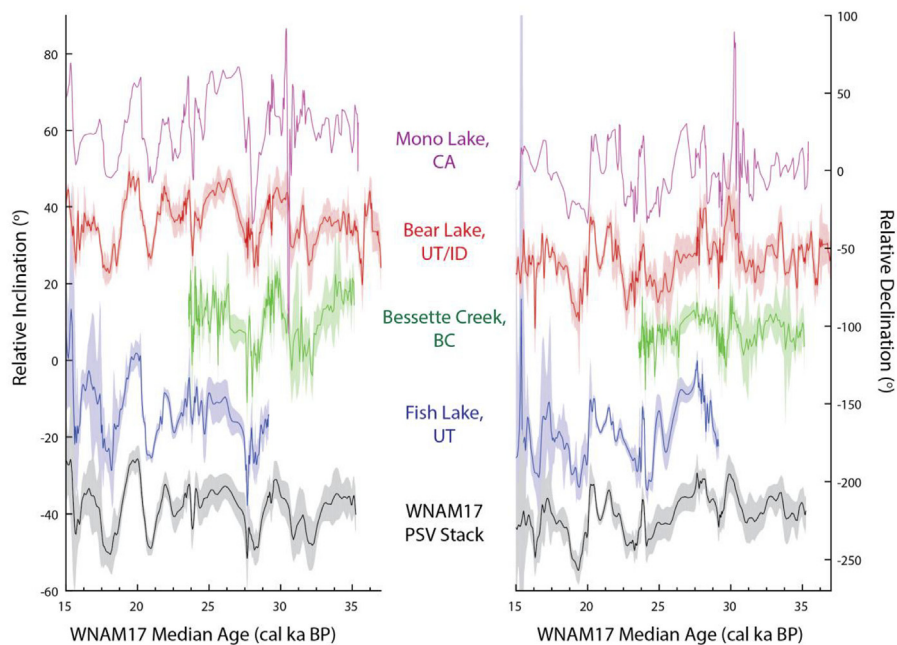


Fig. 12. Western North American PSV records projected to Seattle, WA discussed in the text and the WNAM17 PSV Stack placed on the WNAM17 median age timescale. Mono Lake data are presented on our Scenario 2 age-depth relationship. An age-depth model that gives an older age for the excursion recorded at Mono Lake, Scenario 1, is presented in Fig. 9c.

of the BL00 cores at Bear Lake) and produce a signal similar to the WNAM17 PSV stack with no obvious excursion (Fig. 10c). This exercise assumes that the higher resolution Mono Lake signal better approximates the true geomagnetic signal, for which a smoothed signal is recorded in other lower accumulation rate depositional systems.

Applying 10,000 age-depth model realizations using the age distributions of tie points to the WNAM17 PSV template places the excursion at Mono Lake, defined by the shallowest inclination, between 29.8 and 31.7 cal ka BP with a median age of 30.6 cal ka BP on the IntCal13 timescale (range is 1σ). This estimate is within uncertainty of anomalous directions dated regionally and globally, included basaltic lava groundmass $^{40}\text{Ar}/^{39}\text{Ar}$ estimates from New Zealand (31.6 ± 0.9 ka; Cassata et al., 2008) and the Canary Islands (32 ± 0.5 ka; Kissel et al., 2011) and radiocarbon estimates from total organic carbon near the correlative ash layer in the Pyramid Lake Basin after applying the 0.6 ka suggested reservoir correction (31.4–32.2 cal ka BP; Benson et al., 2003a) and from terrestrial macrofossils in anomalous magnetic directions in a drill core from the Santa Clara Valley (31.5–32.4 cal ka BP; Mankinen and Wentworth, 2004) (Fig. 11). Interestingly, in comparison to the ^{10}Be flux record from Greenland ice cores on the GICC05 timescale (Muscheler et al., 2014), these estimates are all more consistent with relatively high ^{10}Be production period around 31 ka than the larger production episode around 34 ka that has been suggested to be correlative with the Mono Lake excursion (Laj and Kissel, 2015; Wagner et al., 2000). The Mono Lake PSV record is presented on this age model and compared to all the records discussed in this paper in Fig. 12.

In summary, both scenarios are possible, but have different stratigraphic, sedimentological, and magnetic implications when evaluated in the context of the WNAM17 template. In Scenario 1, the age of the excursion would be consistent with the globally recognized Laschamp Excursion (~41 ka) and would be consistent with ^{238}U – ^{230}Th allanite rim dates approximating true eruption ages. However, it is difficult to reconcile the much lower sedimentation rates needed to fit this model without distorting the large amplitude PSV features older than 30 ka and invoking a hiatus or lower/variable accumulation rates complicating the signal. In Scenario 2, the age of the excursion would be consistent with independent age estimates for a shorter duration anomalous geomagnetic event recognized in a few locations between 30 and 32 ka. This scenario implies that sedimentation rates increase in the lithologic unit containing the excursion, approaching ~100 cm/ka or higher, allowing for better preservation of a short duration signal compared to the lower accumulation rate (on the order of 10^1 cm/ka) sites used to build the WNAM17 template. However, this scenario also implies that ^{238}U – ^{230}Th allanite dates are anomalously old for ash layers 11, 15, 17, and 19, but not ash layer 7.

6. Conclusion

We present new PSV and geochronological data from Fish Lake, UT which, when compared and correlated to other regional PSV records, provides improved constraints on the region's PSV signal and the chronology of that signal. This template can be used to address uncertainties in Late Pleistocene Western North American chronologies. In addition to radiocarbon and age modeling uncertainties, we also take into account uncertainties that result from sediment magnetic acquisition processes to develop realistic magnetic age estimates for our regional PSV stack, WNAM17, spanning ~35–15 ka (Fig. 12). We illustrate with two examples that an independently dated regional PSV template can be used to assess chronologic uncertainties in sediments that are otherwise difficult to date. Comparison of the timing of local glacial maxima in

the Bear Lake and Fish Lake, UT Basins using WNAM17 'tuned' chronologies suggest major glacial advances and retreats could be in-phase, in contrast to what is suggested from their independent chronologies. Application of the stack to assess the controversial chronology of Late Pleistocene sediments at Mono Lake, California refines the age model for sediments younger than 25 ka and offers new insight into magnetic, geochronological, and sedimentological implications for the age of the excursion recorded in the Wilson Creek Formation. Specifically, a ~30–34 ka aged excursion would be recorded in high accumulation rate sediments and the WNAM17 and Lund et al. (1988) PSV signals could be reconciled by invoking reasonable smoothing associated with sediment magnetic acquisition processes. Alternatively, a ~41 ka aged excursion would require either low and/or variable accumulation rates that would smooth and/or distort the Wilson Creek Formation PSV signal or an unrecognized hiatus to reconcile the WNAM17 and Lund et al. (1988) PSV signals.

PSV stratigraphy is a powerful tool for assessing the chronologies of Late Pleistocene sediments in Western North America. Our regional chronostratigraphic model allows basin-specific age-depth models that have geologic uncertainties to be evaluated, a problem that is difficult to address otherwise. The WNAM17 PSV template offers a new independently dated and regionally developed tuning target. Moving forward, we can reduce uncertainties through the identification of records with strong chronologies and well-defined PSV even for discrete time intervals and through an improved understanding of sediment magnetic remanence acquisition processes.

Acknowledgements

We are thankful to the 2014 Fish Lake, Utah coring team and working group, particularly Lesleigh Anderson, Andrea Brunelle, Vachel Carter, and Mitchel Power. The 2014 Fish Lake, Utah cores are stored at the OSU Marine and Geology Repository (www.osu-mgr.org; NSF-OCE1558679) and we thank Maziet Cheseby and staff for their help. We thank Jason Wiest and the OSU College of Veterinary Medicine for their help to CT scan these cores. We thank Chanda Bertrand for help with radiocarbon sample preparation and John Southon for radiocarbon measurements. We thank three anonymous reviewers for their constructive and supportive reviews. Brendan Reilly is thankful for support from Leslie and Mark Workman and the ARCS Foundation Oregon Chapter. Funding from NSF-EAR1215888 to Joseph Stoner and NSF-EAR1215661 to Mark Abbott contributed to this product.

Appendix A. Supplementary data

Supplementary data to this article can be found online at <https://doi.org/10.1016/j.quascirev.2018.10.016>.

References

- Abbott, M.B., Stafford, T.W., 1996. Radiocarbon geochemistry of modern and ancient arctic lake systems, Baffin Island, Canada. *Quat. Res.* 45, 300–311. <https://doi.org/10.1006/qres.1996.0031>.
- Bailey, C., Harris, M.S., Marchetti, D.W., 2007. Geologic overview of the Fish Lake plateau, Utah. In: Willis, G.C., Hylland, M.D., Clark, D.L., Chidsey, T.C. (Eds.), *Central Utah - Diverse Geology of a Dynamic Landscape*. Utah Geology Association Publication, pp. 47–55.
- Balbas, A.M., Koppers, A.A.P., Clark, P.U., Coe, R.S., Reilly, B.T., Stoner, J.S., Konrad, K., 2018. Millennial-scale instability in the geomagnetic field prior to the Matuyama-Brunhes reversal. *Geochem. Geophys. Geosystems* 19, 952–967. <https://doi.org/10.1002/2017GC007404>.
- Barletta, F., St-Onge, G., Channell, J.E.T., Rochon, A., Polyak, L., Darby, D., 2008. High-resolution paleomagnetic secular variation and relative paleointensity records from the western Canadian Arctic: implications for Holocene stratigraphy and geomagnetic field behaviour. *Can. J. Earth Sci.* 45, 1265–1281. <https://doi.org/10.1139/E08-011>.

- 1139/E08-039.
- Barletta, F., St-Onge, G., Stoner, J.S., Lajeunesse, P., Locat, J., 2010. A high-resolution Holocene paleomagnetic secular variation and relative paleointensity stack from eastern Canada. *Earth Planet. Sci. Lett.* 298, 162–174. <https://doi.org/10.1016/j.epsl.2010.07.038>.
- Benson, L., Liddicoat, J., Smoot, J., Sarna-Wojcicki, A., Negrini, R., Lund, S., 2003a. Age of the Mono Lake excursion and associated tephra. *Quat. Sci. Rev.* 22, 135–140. [https://doi.org/10.1016/S0277-3791\(02\)00249-4](https://doi.org/10.1016/S0277-3791(02)00249-4).
- Benson, L., Lund, S., Negrini, R., Linsley, B., Zic, M., 2003b. Response of North American great basin lakes to Dansgaard–Oeschger oscillations. *Quat. Sci. Rev.* 22, 2239–2251. [https://doi.org/10.1016/S0277-3791\(03\)00210-5](https://doi.org/10.1016/S0277-3791(03)00210-5).
- Benson, L.V., Currey, D.R., Dorn, R.I., Lajoie, K.R., Oviatt, C.G., Robinson, S.W., Smith, G.I., Stine, S., 1990. Chronology of expansion and contraction of four Great Basin lake systems during the past 35,000 years. *Palaeogeogr. Palaeoclimatol. Palaeoecol.* 78, 241–286.
- Benson, L.V., Lund, S.P., Burdett, J.W., Kashgarian, M., Rose, T.P., Smoot, J.P., Schwartz, M., 1998. Correlation of late-Pleistocene lake-level oscillations in Mono Lake, California, with North Atlantic climate events. *Quat. Res.* 49, 1–10. <https://doi.org/10.1006/qres.1997.1940>.
- Benson, L.V., Lund, S.P., Smoot, J.P., Rhode, D.E., Spencer, R.J., Verosub, K.L., Louderback, L.A., Johnson, C.A., Rye, R.O., Negrini, R.M., 2011. The rise and fall of Lake Bonneville between 45 and 10.5 ka. *Quat. Int.* 235, 57–69. <https://doi.org/10.1016/j.quaint.2010.12.014>.
- Blanchet, C.L., Thouveny, N., Vidal, L., Leduc, G., Tachikawa, K., Bard, E., Beaufort, L., 2007. Terrigenous input response to glacial/interglacial climatic variations over southern Baja California: a rock magnetic approach. *Quat. Sci. Rev.* 26, 3118–3133. <https://doi.org/10.1016/j.quascirev.2007.07.008>.
- Bloxham, J., 2002. Time-independent and time-dependent behaviour of high-latitude flux bundles at the core-mantle boundary. *Geophys. Res. Lett.* 29, 1854. <https://doi.org/10.1029/2001GL014543>.
- Brachfeld, S.A., Banerjee, S.K., 2000. A new high-resolution geomagnetic relative paleointensity record for the North American Holocene: a comparison of sedimentary and absolute intensity data. *J. Geophys. Res. Solid Earth* 105, 821–834. <https://doi.org/10.1029/1999JB900365>.
- Broecker, W.S., Wanninkhof, R., Mathieu, G., Peng, T.-H., Stine, S., Robinson, S., Herczeg, A., Stuiver, M., 1988. The radiocarbon budget for Mono Lake: an unsolved mystery. *Earth Planet. Sci. Lett.* 88, 16–26. [https://doi.org/10.1016/0012-821X\(88\)90042-8](https://doi.org/10.1016/0012-821X(88)90042-8).
- Cassata, W.S., Singer, B.S., Cassidy, J., 2008. Laschamp and Mono Lake geomagnetic excursions recorded in New Zealand. *Earth Planet. Sci. Lett.* 268, 76–88. <https://doi.org/10.1016/j.epsl.2008.01.009>.
- Cassata, W.S., Singer, B.S., Liddicoat, J.C., Coe, R.S., 2010. Reconciling discrepant chronologies for the geomagnetic excursion in the Mono Basin, California: insights from new ⁴⁰Ar/³⁹Ar dating experiments and a revised relative paleointensity correlation. *Quat. Geochronol.* 5, 533–543. <https://doi.org/10.1016/j.quageo.2010.02.001>.
- Channell, J. e. t., 2017. Mid-Brunhes magnetic excursions in marine isotope stages 9, 13, 14, and 15 (286, 495, 540, and 590 ka) at North Atlantic IODP Sites U1302/3, U1305 and U1306. *Geochem. Geophys. Geosys. n/a-n/a* <https://doi.org/10.1002/2016GC006626>.
- Channell, J.E.T., Guyodo, Y., 2004. The Matuyama chronozone at ODP site 982 (Rockall Bank): evidence for decimeter-scale magnetization lock-in depths. In: Channell, J.E.T., Kent, D.V., Lowrie, W., Meert, J.G. (Eds.), *Timescales of the Paleomagnetic Field*. American Geophysical Union, pp. 205–219.
- Clague, J.J., Barendregt, R., Enkin, R.J., Foit, F.F., 2003. Paleomagnetic and tephra evidence for tens of Missoula floods in southern Washington. *Geology* 31, 247–250. [https://doi.org/10.1130/0091-7613\(2003\)031%3C0247:PATEFT%3e2.0.CO;2](https://doi.org/10.1130/0091-7613(2003)031%3C0247:PATEFT%3e2.0.CO;2).
- Colman, S.M., Kaufman, D.S., Bright, J., Heil, C., King, J.W., Dean, W.E., Rosenbaum, J.G., Forester, R.M., Bischoff, J.L., Perkins, M., McGeehin, J.P., 2006. Age model for a continuous, ca 250-ka Quaternary lacustrine record from Bear Lake, Utah–Idaho. *Quat. Sci. Rev.* 25, 2271–2282. <https://doi.org/10.1016/j.quascirev.2005.10.015>.
- Colman, S.M., Rosenbaum, J.G., Kaufman, D.S., Dean, W.E., McGeehin, J.P., 2009. Radiocarbon ages and age models for the past 30,000 years in Bear Lake, Utah and Idaho. *Geol. Soc. Am. Spec. Pap.* 450, 133–144. [https://doi.org/10.1130/2009.2450\(05\)](https://doi.org/10.1130/2009.2450(05)).
- Cox, S.E., Fairley, K.A., Hemming, S.R., 2012. Insights into the age of the Mono Lake Excursion and magmatic crystal residence time from (U-Th)/He and ²³⁰Th dating of volcanic allanite. *Earth Planet. Sci. Lett.* 319–320, 178–184. <https://doi.org/10.1016/j.epsl.2011.12.025>.
- Darby, D.A., Ortiz, J.D., Grosch, C.E., Lund, S.P., 2012. 1,500-year cycle in the Arctic Oscillation identified in Holocene Arctic sea-ice drift. *Nat. Geosci.* 5, 897–900. <https://doi.org/10.1038/ngeo1629>.
- deMenocal, P.B., Ruddiman, W.F., Kent, D.V., 1990. Depth of post-depositional remanence acquisition in deep-sea sediments: a case study of the Brunhes–Matuyama reversal and oxygen isotopic Stage 19.1. *Earth Planet. Sci. Lett.* 99, 1–13. [https://doi.org/10.1016/0012-821X\(90\)90066-7](https://doi.org/10.1016/0012-821X(90)90066-7).
- Denham, C.R., Cox, A., 1971. Evidence that the Laschamp polarity event did not occur 13 300–400 years ago. *Earth Planet. Sci. Lett.* 13, 181–190.
- Donadini, F., Korte, M., Constable, C.G., 2009. Geomagnetic field for 0–3 ka: 1. New data sets for global modeling. *Geochem. Geophys. Geosystems* 10, Q06007. <https://doi.org/10.1029/2008GC002295>.
- Egli, R., Zhao, X., 2015. Natural remanent magnetization acquisition in bioturbated sediment: general theory and implications for relative paleointensity reconstructions: initial NRM acquisition in sediment. *Geochem. Geophys. Geosystems* 16, 995–1016. <https://doi.org/10.1002/2014GC005672>.
- Fisher, R., 1953. Dispersion on a sphere. *Proc. Natl. Acad. Sci. U. S. Am. Math. Phys. Sci.* 217, 295–305.
- Hagstrum, J.T., Blinman, E., 2010. Archeomagnetic dating in western North America: an updated reference curve based on paleomagnetic and archeomagnetic data sets. *Geochem. Geophys. Geosystems* 11, Q06009. <https://doi.org/10.1029/2009GC002979>.
- Hagstrum, J.T., Champion, D.E., 2002. A Holocene paleosecular variation record from 14C-dated volcanic rocks in western North America. *J. Geophys. Res.* 107. <https://doi.org/10.1029/2001JB000524>.
- Hajdas, I., Bonani, G., Zimmerman, S.H., Mendels, M., Hemming, S., 2004. 14C ages of ostracodes from Pleistocene lake sediments of the western Great Basin, USA: results of progressive acid leaching. *Radiocarbon* 46, 189–200.
- Hanna, R.L., Verosub, K.L., 1989. A review of lacustrine paleomagnetic records from western North America: 0–40000 years BP. *Phys. Earth Planet. In.* 56, 76–95. [https://doi.org/10.1016/0031-9201\(89\)90038-1](https://doi.org/10.1016/0031-9201(89)90038-1).
- Hanna, R.L., Verosub, K.L., 1988. A 3500-year paleomagnetic record of Late Holocene secular variation from Blue Lake, Idaho. *Geophys. Res. Lett.* 15, 685–688. <https://doi.org/10.1029/GL015i007p00685>.
- Haslett, J., Parnell, A., 2008. A simple monotone process with application to radiocarbon-dated depth chronologies. *J. R. Stat. Soc. Ser. C Appl. Stat.* 57, 399–418. <https://doi.org/10.1111/j.1467-9876.2008.00623.x>.
- Heil, C.W., King, J.W., Rosenbaum, J.G., Reynolds, R.L., Colman, S.M., 2009. Paleomagnetism and environmental magnetism of GLAD800 sediment cores from Bear Lake, Utah and Idaho. *Geol. Soc. Am. Spec. Pap.* 450, 291–310. [https://doi.org/10.1130/2009.2450\(13\)](https://doi.org/10.1130/2009.2450(13)).
- Howarth, J.D., Fitzsimons, S.J., Jacobsen, G.E., Vandergoes, M.J., Norris, R.J., 2013. Identifying a reliable target fraction for radiocarbon dating sedimentary records from lakes. *Quat. Geochronol.* 17, 68–80. <https://doi.org/10.1016/j.quageo.2013.02.001>.
- Irving, E., Major, A., 1964. Post-depositional detrital remanent magnetization in a synthetic sediment. *Sedimentology* 3, 135–143. <https://doi.org/10.1111/j.1365-3091.1964.tb00638.x>.
- Jackson, A., Jonkers, A.R., Walker, M.R., 2000. Four centuries of geomagnetic secular variation from historical records. *Philos. Trans. R. Soc. Lond. Math. Phys. Eng. Sci.* 358, 957–990.
- Jackson, M., Bowles, J.A., Lascu, I., Solheid, P., 2010. Deconvolution of u channel magnetometer data: experimental study of accuracy, resolution, and stability of different inversion methods. *Geochem. Geophys. Geosystems* 11, Q07Y10. <https://doi.org/10.1029/2009GC002991>.
- Johnson, C.L., McFadden, P., 2007. Time-averaged field and paleosecular variation. In: Schubert, G. (Ed.), *Treatise on Geophysics*. Elsevier, Amsterdam, pp. 417–453. <https://doi.org/10.1016/B978-0-44452748-6.00096-1>.
- Kaufman, D.S., Bright, J., Dean, W.E., Rosenbaum, J.G., Moser, K., Anderson, R.S., Colman, S.M., Heil, C.W., Jiménez-Moreno, G., Reheis, M.C., Simmons, K.R., 2009. A quarter-million years of paleoenvironmental change at Bear Lake, Utah and Idaho. *Geol. Soc. Am. Spec. Pap.* 450, 311–351. [https://doi.org/10.1130/2009.2450\(14\)](https://doi.org/10.1130/2009.2450(14)).
- Kent, D.V., Hemming, S.R., Turrin, B.D., 2002. Laschamp excursion at Mono Lake? *Earth Planet. Sci. Lett.* 197, 151–164. [https://doi.org/10.1016/S0012-821X\(02\)00474-0](https://doi.org/10.1016/S0012-821X(02)00474-0).
- Khokhlov, A., Hulot, G., 2016. Principal component analysis of palaeomagnetic directions: converting a Maximum Angular Deviation (MAD) into an α_{95} angle. *Geophys. J. Int.* 204, 274–291. <https://doi.org/10.1093/gji/ggv451>.
- Kirschvink, J.L., 1980. The least-squares line and plane and the analysis of palaeomagnetic data. *Geophys. J. Roy. Astron. Soc.* 62, 699–718.
- Kissel, C., Guillou, H., Laj, C., Carracedo, J.C., Nomade, S., Perez-Torrado, F., Wandres, C., 2011. The Mono Lake excursion recorded in phonolitic lavas from Tenerife (Canary Islands): paleomagnetic analyses and coupled K/Ar and Ar/Ar dating. *Phys. Earth Planet. Inter., Special Issue: Planetary Magnetism, Dynamo and Dynamics* 187, 232–244. <https://doi.org/10.1016/j.pepi.2011.04.014>.
- Kuehn, S.C., 2016. Routine EPMA of silicate glasses using a 5 micron beam: taking advantage of TDI, combined EDS+WDS, MAN, and a multi-standard blank correction. In: EPMA 2016 Topical Conference Program Guide with Abstracts. Presented at the EMPA 2016 Topical Conference, Madison, WI, pp. 40–41. <https://doi.org/10.13140/RG.2.1.2656.0882>.
- Kuehn, S.C., Froese, D.G., Shane, P.A.R., 2011. The INTAV intercomparison of electron-beam microanalysis of glass by tephrochronology laboratories: results and recommendations. *Quat. Int.* 246, 19–47. Enhancing tephrochronology and its application (INTREPID Project): Hiroshi Machida commemorative volume. <https://doi.org/10.1016/j.quaint.2011.08.022>.
- Laj, C., Guillou, H., Kissel, C., 2014. Dynamics of the earth magnetic field in the 10–75 kyr period comprising the Laschamp and Mono Lake excursions: new results from the French Chaîne des Puys in a global perspective. *Earth Planet. Sci. Lett.* 387, 184–197. <https://doi.org/10.1016/j.epsl.2013.11.031>.
- Laj, C., Kissel, C., 2015. An impending geomagnetic transition? Hints from the past. *Geomagn. Paleomagn.* 61. <https://doi.org/10.3389/feart.2015.00061>.
- Laj, C., Kissel, C., Beer, J., 2004. High resolution global paleointensity stack since 75 kyr (GLOPI5-75) calibrated to absolute values. In: Channell, J.E.T., Kent, D.V., Lowrie, W., Meert, J.G. (Eds.), *Timescales of the Paleomagnetic Field*. American Geophysical Union, pp. 255–265.
- Lascu, I., Feinberg, J.M., Dorale, J.A., Cheng, H., Edwards, R.L., 2016. Age of the Laschamp excursion determined by U-Th dating of a speleothem geomagnetic record from North America. *Geology* 44, 139–142. <https://doi.org/10.1130/>

- G37490.1.
- Liddicoat, J.C., 1992. Mono Lake excursion in Mono Basin, California, and at Carson Sink and Pyramid Lake, Nevada. *Geophys. J. Int.* 108, 442–452. <https://doi.org/10.1111/j.1365-246X.1992.tb04627.x>.
- Liddicoat, J.C., Coe, R.S., 1979. Mono Lake geomagnetic excursion. *J. Geophys. Res. Solid Earth* 84, 261–271. <https://doi.org/10.1029/JB084iB01p00261>.
- Lougheed, B., Obrochta, S., 2016. MatCal: open source Bayesian ¹⁴C age calibration in matlab. *J. Open Res. Software* 4. <https://doi.org/10.5334/jors.130>.
- Lougheed, B.C., Nilsson, A., Björck, S., Snowball, I., Muscheler, R., 2014. A deglacial palaeomagnetic master curve for Fennoscandia – providing a dating template and supporting millennial-scale geomagnetic field patterns for the past 14 ka. *Quat. Sci. Rev.* 106, 155–166. Dating, Synthesis, and Interpretation of Palaeoclimatic Records and Model-data Integration: Advances of the INTIMATE project (INTEgration of Ice core, Marine and Terrestrial records, COST Action ES0907). <https://doi.org/10.1016/j.quascirev.2014.03.008>.
- Løvlie, R., 1976. The intensity pattern of post-depositional remanence acquired in some marine sediments deposited during a reversal of the external magnetic field. *Earth Planet Sci. Lett.* 30, 209–214. [https://doi.org/10.1016/0012-821X\(76\)90247-8](https://doi.org/10.1016/0012-821X(76)90247-8).
- Lund, S., Benson, L., Negrini, R., Liddicoat, J., Mensing, S., 2017. A full-vector paleomagnetic secular variation record (PSV) from Pyramid Lake (Nevada) from 47–17 ka: evidence for the successive Mono Lake and Laschamp Excursions. *Earth Planet Sci. Lett.* 458, 120–129. <https://doi.org/10.1016/j.epsl.2016.09.036>.
- Lund, S.P., 2007. Paleomagnetic secular variation. In: Gubbins, D., Herrero-Bervera, E. (Eds.), *Encyclopedia of Geomagnetism and Paleomagnetism*. Springer Netherlands, pp. 766–776. https://doi.org/10.1007/978-1-4020-4423-6_255.
- Lund, S.P., 1996. A comparison of Holocene paleomagnetic secular variation records from North America. *J. Geophys. Res. Solid Earth* 101, 8007–8024. <https://doi.org/10.1029/95JB00039>.
- Lund, S.P., Keigwin, L., 1994. Measurement of the degree of smoothing in sediment paleomagnetic secular variation records: an example from late Quaternary deep-sea sediments of the Bermuda Rise, western North Atlantic Ocean. *Earth Planet Sci. Lett.* 122, 317–330. [https://doi.org/10.1016/0012-821X\(94\)90005-1](https://doi.org/10.1016/0012-821X(94)90005-1).
- Lund, S.P., Liddicoat, J.C., Lajoie, K.R., Henyey, T.L., Robinson, S.W., 1988. Paleomagnetic evidence for long-term (10⁴ year) Memory and periodic behavior in the Earth's core dynamo process. *Geophys. Res. Lett.* 15, 1101–1104. <https://doi.org/10.1029/GL015i010p01101>.
- Maier, B.A., 1988. Magnetic properties of some synthetic sub-micron magnetites. *Geophys. J. Int.* 94, 83–96. <https://doi.org/10.1111/j.1365-246X.1988.tb03429.x>.
- Mankinen, E.A., Wentworth, C.M., 2004. Mono Lake excursion recorded in sediment of the Santa Clara Valley, California. *Geochem. Geophys. Geosystems* 5, Q02H05. <https://doi.org/10.1029/2003GC000592>.
- Marchetti, D.W., Harris, M.S., Bailey, C.M., Cerling, T.E., Bergman, S., 2011. Timing of glaciation and last glacial maximum paleoclimate estimates from the Fish Lake Plateau, Utah. *Quat. Res.* 75, 183–195. <https://doi.org/10.1016/j.yqres.2010.09.009>.
- Mazaud, A., 2006. A first-order correction to minimize environmental influence in sedimentary records of relative paleointensity of the geomagnetic field. *Geochem. Geophys. Geosystems* 7, Q07002. <https://doi.org/10.1029/2006GC001257>.
- Mellström, A., Nilsson, A., Stanton, T., Muscheler, R., Snowball, I., Suttie, N., 2015. Post-depositional remanent magnetization lock-in depth in precisely dated varved sediments assessed by archaeomagnetic field models. *Earth Planet Sci. Lett.* 410, 186–196. <https://doi.org/10.1016/j.epsl.2014.11.016>.
- Muscheler, R., Adolphi, F., Svensson, A., 2014. Challenges in ¹⁴C dating towards the limit of the method inferred from anchoring a floating tree ring radiocarbon chronology to ice core records around the Laschamp geomagnetic field minimum. *Earth Planet Sci. Lett.* 394, 209–215. <https://doi.org/10.1016/j.epsl.2014.03.024>.
- Negrini, R.M., Davis, J.O., Verosub, K.L., 1984. Mono Lake geomagnetic excursion found at summer lake, Oregon. *Geology* 12, 643–646. [https://doi.org/10.1130/0091-7613\(1984\)12%3c643:MLGEFA%3e2.0.CO;2](https://doi.org/10.1130/0091-7613(1984)12%3c643:MLGEFA%3e2.0.CO;2).
- Negrini, R.M., McCuan, D.T., Horton, R.A., Lopez, J.D., Cassata, W.S., Channell, J.E.T., Verosub, K.L., Knott, J.R., Coe, R.S., Liddicoat, J.C., Lund, S.P., Benson, L.V., Sarna-Wojcicki, A.M., 2014. Nongeo-centric axial dipole field behavior during the Mono Lake excursion. *J. Geophys. Res. Solid Earth* 119, 2567–2581. <https://doi.org/10.1002/2013JB010846>.
- Nilsson, A., Holme, R., Korte, M., Suttie, N., Hill, M., 2014. Reconstructing Holocene geomagnetic field variation: new methods, models and implications. *Geophys. J. Int.* 198, 229–248. <https://doi.org/10.1093/gji/ggu120>.
- Nilsson, A., Muscheler, R., Snowball, I., 2011. Millennial scale cyclicity in the geodynamo inferred from a dipole tilt reconstruction. *Earth Planet Sci. Lett.* 311, 299–305. <https://doi.org/10.1016/j.epsl.2011.09.030>.
- Nilsson, A., Snowball, I., Muscheler, R., Uvo, C.B., 2010. Holocene geocentric dipole tilt model constrained by sedimentary paleomagnetic data. *Geochem. Geophys. Geosystems* 11. <https://doi.org/10.1029/2010GC003118>.
- Nilsson, A., Suttie, N., Hill, M.J., 2018. Short-term magnetic field variations from the post-depositional remanence of lake sediments. *Front. Earth Sci.* 6. <https://doi.org/10.3389/feart.2018.00039>.
- Nowaczyk, N.R., Arz, H.W., Frank, U., Kind, J., Plessen, B., 2012. Dynamics of the Laschamp geomagnetic excursion from Black Sea sediments. *Earth Planet Sci. Lett.* 351–352, 54–69. <https://doi.org/10.1016/j.epsl.2012.06.050>.
- Nowaczyk, N.R., Frank, U., Kind, J., Arz, H.W., 2013. A high-resolution paleointensity stack of the past 14 to 68 ka from Black Sea sediments. *Earth Planet Sci. Lett.* 384, 1–16. <https://doi.org/10.1016/j.epsl.2013.09.028>.
- Oberg, C.J., Evans, M.E., 1977. Spectral analysis of Quaternary palaeomagnetic data from British Columbia and its bearing on geomagnetic secular variation. *Geophys. J. Int.* 51, 691–699. <https://doi.org/10.1111/j.1365-246X.1977.tb04214.x>.
- Oda, H., Shibuya, H., 1996. Deconvolution of long-core paleomagnetic data of ocean drilling program by Akaike's Bayesian information criterion minimization. *J. Geophys. Res. Solid Earth* 101, 2815–2834. <https://doi.org/10.1029/95JB02811>.
- Oda, H., Xuan, C., 2014. Deconvolution of continuous paleomagnetic data from pass-through magnetometer: a new algorithm to restore geomagnetic and environmental information based on realistic optimization. *Geochem. Geophys. Geosystems* 15, 3907–3924. <https://doi.org/10.1002/2014GC005513>.
- Ólafsdóttir, S., Geirsdóttir, A., Miller, G.H., Stoner, J.S., Channell, J.E.T., 2013. Synchronizing Holocene lacustrine and marine sediment records using paleomagnetic secular variation. *Geology* 41, 535–538. <https://doi.org/10.1130/G33946.1>.
- Oviatt, C.G., Nash, B.P., 2014. The Pony Express Basaltic Ash: a Stratigraphic Marker in Lake Bonneville Sediments. *Miscellaneous Publications. Utah Geological Survey, Utah*.
- Oviatt, C.G., Nash, W.P., 1989. Late Pleistocene basaltic ash and volcanic eruptions in the Bonneville basin, Utah. *Geol. Soc. Am. Bull.* 101, 292–303. [https://doi.org/10.1130/0016-7606\(1989\)101%3c0292:LPBAAV%3e2.3.CO;2](https://doi.org/10.1130/0016-7606(1989)101%3c0292:LPBAAV%3e2.3.CO;2).
- Reilly, B.T., Stoner, J.S., Wiest, J., 2017. SedCT: MATLAB™ tools for standardized and quantitative processing of sediment core computed tomography (CT) data collected using a medical CT scanner. *Geochem. Geophys. Geosystems* 18, 3231–3240. <https://doi.org/10.1002/2017GC006884>.
- Reimer, P.J., Bard, E., Bayliss, A., Beck, J.W., Blackwell, P.G., Ramsey, C.B., Buck, C.E., Cheng, H., Edwards, R.L., Friedrich, M., Grootes, P.M., Guilderson, T.P., Hafliðason, H., Hajdas, I., Hatté, C., Heaton, T.J., Hoffmann, D.L., Hogg, A.G., Hughen, K.A., Kaiser, K.F., Kromer, B., Manning, S.W., Niu, M., Reimer, R.W., Richards, D.A., Scott, E.M., Southon, J.R., Staff, R.A., Turney, C.S.M., Plicht, van der, J., 2013. IntCal13 and Marine13 radiocarbon age calibration curves 0–50,000 Years cal BP. *Radiocarbon* 55, 1869–1887. https://doi.org/10.2458/azu_js_rc.55.16947.
- Rosenbaum, J.G., Heil, C.W., 2009. The glacial/deglaial history of sedimentation in Bear Lake, Utah and Idaho. *Spec. Pap. Geol. Soc. Am.* 15. <https://doi.org/10.1130/2009.2450.11>.
- Schwartz, M., Lund, S., Johnson, T., 1996. Environmental factors as complicating influences in the recovery of quantitative geomagnetic-field paleointensity estimates from sediments. *Geophys. Res. Lett.* 23, 2693–2696. <https://doi.org/10.1029/96GL02375>.
- Simon, Q., Bourlès, D.L., Thouveny, N., Hornig, C.-S., Valet, J.-P., Bassinot, F., Choy, S., 2018. Cosmogenic signature of geomagnetic reversals and excursions from the Réunion event to the Matuyama–Brunhes transition (0.7–2.14 Ma interval). *Earth Planet Sci. Lett.* 482, 510–524. <https://doi.org/10.1016/j.epsl.2017.11.021>.
- Singer, B.S., 2014. A Quaternary geomagnetic instability time scale. *Quat. Geochronol.* 21, 29–52. <https://doi.org/10.1016/j.quageo.2013.10.003>.
- Snowball, I., Mellström, A., Ahlstrand, E., Haltia, E., Nilsson, A., Ning, W., Muscheler, R., Brauer, A., 2013. An estimate of post-depositional remanent magnetization lock-in depth in organic rich varved lake sediments. *Glob. Planet. Change, Magnetic iron minerals in sediments and their relation to geologic processes, climate, and the geomagnetic field* 110, 264–277. <https://doi.org/10.1016/j.gloplacha.2013.10.005>.
- Snowball, I., Zillén, L., Ojala, A., Saarinen, T., Sandgren, P., 2007. FENNOSTACK and FENNORPIS: varve dated Holocene paleomagnetic secular variation and relative paleointensity stacks for Fennoscandia. *Earth Planet Sci. Lett.* 255, 106–116. <https://doi.org/10.1016/j.epsl.2006.12.009>.
- Stoner, J.S., Channell, J.E.T., Mazaud, A., Strano, S.E., Xuan, C., 2013. The influence of high-latitude flux lobes on the Holocene paleomagnetic record of IODP Site U1305 and the northern North Atlantic. *Geochem. Geophys. Geosystems* 14, 4623–4646. <https://doi.org/10.1002/ggge.20272>.
- Stoner, J.S., Jennings, A., Kristjánsson, G.B., Dunhill, G., Andrews, J.T., Hardardóttir, J., 2007. A paleomagnetic approach toward refining Holocene radiocarbon-based chronologies: paleoceanographic records from the north Iceland (MD99-2269) and east Greenland (MD99-2322) margins. *Paleoceanography* 22. <https://doi.org/10.1029/2006PA001285>.
- Stoner, J.S., Laj, C., Channell, J.E.T., Kissel, C., 2002. South Atlantic and North Atlantic geomagnetic paleointensity stacks (0–80ka): implications for inter-hemispheric correlation. *Quat. Sci. Rev.* 21, 1141–1151.
- Stoner, J.S., St-Onge, G., 2007. Chapter three magnetic stratigraphy in paleoceanography: reversals, excursions, paleointensity, and secular variation. In: *Developments in Marine Geology*. Elsevier, pp. 99–138.
- St-Onge, G., Stoner, J., 2011. Paleomagnetism near the North magnetic pole: a unique vantage point for understanding the dynamics of the geomagnetic field and its secular variations. *Oceanography* 24, 42–50. <https://doi.org/10.5670/oceanog.2011.53>.
- Suganuma, Y., Yokoyama, Y., Yamazaki, T., Kawamura, K., Hornig, C.-S., Matsuzaki, H., 2010. ¹⁰Be evidence for delayed acquisition of remanent magnetization in marine sediments: implication for a new age for the Matuyama–Brunhes boundary. *Earth Planet Sci. Lett.* 296, 443–450. <https://doi.org/10.1016/j.epsl.2010.05.031>.
- Tauxe, L., 1993. Sedimentary records of relative paleointensity of the geomagnetic field: theory and practice. *Rev. Geophys.* 31, 319–354.
- Thompson, R., Turner, G.M., 1979. British geomagnetic master curve 10,000-0 yr B.P. for dating European sediments. *Geophys. Res. Lett.* 6, 249–252.
- Turner, G.M., Evans, M.E., Hussin, I.B., 1982. A geomagnetic secular variation study (31000–19 500 bp) in Western Canada. *Geophys. J. Int.* 71, 159–171. <https://doi.org/10.1111/j.1365-246X.1982.tb00421.x>.

- [org/10.1111/j.1365-246X.1982.tb04990.x](https://doi.org/10.1111/j.1365-246X.1982.tb04990.x).
- Valet, J.-P., Bassinot, F., Bouilloux, A., Bourlès, D., Nomade, S., Guillou, V., Lopes, F., Thouveny, N., Dewilde, F., 2014. Geomagnetic, cosmogenic and climatic changes across the last geomagnetic reversal from Equatorial Indian Ocean sediments. *Earth Planet Sci. Lett.* 397, 67–79. <https://doi.org/10.1016/j.epsl.2014.03.053>.
- Valet, J.-P., Fournier, A., 2016. Deciphering records of geomagnetic reversals. *Rev. Geophys.* 54, 410–446. <https://doi.org/10.1002/2015RG000506>.
- Vazquez, J.A., Lidzbarski, M.I., 2012. High-resolution tephrochronology of the Wilson Creek Formation (Mono Lake, California) and Laschamp event using 238U–230Th SIMS dating of accessory mineral rims. *Earth Planet Sci. Lett.* 357–358, 54–67. <https://doi.org/10.1016/j.epsl.2012.09.013>.
- Verosub, K.L., 1977. Depositional and postdepositional processes in the magnetization of sediments. *Rev. Geophys.* 15, 129–143. <https://doi.org/10.1029/RG015i002p00129>.
- Verosub, K.L., Mehringer, P.J., Waterstraat, P., 1986. Holocene secular variation in western North America: paleomagnetic record from Fish Lake, Harney County, Oregon. *J. Geophys. Res.* 91, 3609–3623.
- Wagner, G., Beer, J., Laj, C., Kissel, C., Masarik, J., Muscheler, R., Sval, H.-A., 2000. Chlorine-36 evidence for the Mono Lake event in the Summit GRIP ice core. *Earth Planet Sci. Lett.* 181, 1–6. [https://doi.org/10.1016/S0012-821X\(00\)00196-5](https://doi.org/10.1016/S0012-821X(00)00196-5).
- Walczak, M.H., Stoner, J.S., Mix, A.C., Jaeger, J., Rosen, G.P., Channell, J.E.T., Heslop, D., Xuan, C., 2017. A 17,000 yr paleomagnetic secular variation record from the southeast Alaskan margin: regional and global correlations. *Earth Planet Sci. Lett.* 473, 177–189. <https://doi.org/10.1016/j.epsl.2017.05.022>.
- Westgate, J.A., Fulton, R.J., 1975. Tephrostratigraphy of Olympia interglacial sediments in south-central British Columbia, Canada. *Can. J. Earth Sci.* 12, 489–502. <https://doi.org/10.1139/e75-042>.
- Wündsche, M., Haberzettl, T., Meadows, M.E., Kirsten, K.L., Kasper, T., Baade, J., Daut, G., Stoner, J.S., Mäusbacher, R., 2016. The impact of changing reservoir effects on the 14C chronology of a Holocene sediment record from South Africa. *Quat. Geochronol.* 36, 148–160. <https://doi.org/10.1016/j.quageo.2016.08.011>.
- Xuan, C., Channell, J.E.T., 2009. UPmag: MATLAB software for viewing and processing u channel or other pass-through paleomagnetic data. *Geochem. Geophys. Geosystems* 10. <https://doi.org/10.1029/2009GC002584>.
- Xuan, C., Oda, H., 2015. UDECOR: deconvolution optimization software for restoring high-resolution records from pass-through paleomagnetic measurements. *Earth Planets Space* 67, 1–17. <https://doi.org/10.1186/s40623-015-0332-x>.
- Zheng, Y., Zheng, H., Deng, C., Liu, Q., 2014. Holocene paleomagnetic secular variation from east China sea and a PSV stack of east Asia. *Phys. Earth Planet. In.* 236, 69–78. <https://doi.org/10.1016/j.pepi.2014.07.001>.
- Zijderveld, J.D.A., 1967. AC demagnetization of rocks: analysis of results. *Methods Paleomagn* 1, 254–286.
- Zimmerman, S.H., Hemming, S.R., Kent, D.V., Searle, S.Y., 2006. Revised chronology for late Pleistocene Mono Lake sediments based on paleointensity correlation to the global reference curve. *Earth Planet Sci. Lett.* 252, 94–106. <https://doi.org/10.1016/j.epsl.2006.09.030>.
- Zimmerman, S.R.H., Hemming, S.R., Hemming, N.G., Tomascak, P.B., Pearl, C., 2011a. High-resolution chemostratigraphic record of late Pleistocene lake-level variability, Mono Lake, California. *Geol. Soc. Am. Bull.* 123, 2320–2334. <https://doi.org/10.1130/B30377.1>.
- Zimmerman, S.R.H., Pearl, C., Hemming, S.R., Tamulonis, K., Hemming, N.G., Searle, S.Y., 2011b. Freshwater control of ice-rafted debris in the last glacial period at Mono Lake, California, USA. *Quat. Res.* 76, 264–271. <https://doi.org/10.1016/j.yqres.2011.06.003>.